An Inverse Mapping Table Method for Raindrop Size Distribution Parameters Retrieval Using X-band Dual-Polarization Radar Observations

Yue Sun, Hui Xiao, Huiling Yang, Liang Feng, Haonan Chen, *Member, IEEE*, and Li Luo

***Abstract*— An inverse mapping table (IMT) method is proposed in this article to retrieve the raindrop size distribution (RSD) parameters from X-band polarimetric weather radar data. In the IMT method, a forward mapping database from three parameters of a gamma-type RSD to polarimetric radar variables is first built based on the scattering simulations under ideal atmospheric conditions, and then an inverse mapping database is derived. In particular, given a fixed shape parameter (μ) of RSD, the intersection of horizontal reflectivity (Z_{H}) and differential reflectivity (Z_{DR}) contour lines is first obtained in the domain of total number concentration (N_{T}) and median volume diameter (MVD) D_0; and the inverse mapping relationship between Z_H and Z_{DR} to N_T and D_0 at a fixed μ value is derived to form a single layer of IMT. Then, the monotonic relationship between μ and the specific differential propagation phase shift (K_{DP}) or backscatter differential phase (δ_{CO}) can aid in determining μ and a single layer of IMT. Thus, the inverse mapping database from polarimetric observations to the three gamma-type RSD parameters μ, N_{T}, and D_0 can be established. Demonstration studies during a convective rainfall event and a large-scale rainfall event which occurred in northeastern China are carried out to examine the performance of this IMT method compared to a constrained-gamma (C-G) method that uses empirical relations between RSD parameters. The results show that the IMT method has a better performance in the convective case and similar performance in the large-scale continuous rainfall case.**

Manuscript received August 14, 2019; revised January 25, 2020; accepted March 6, 2020. Date of publication April 10, 2020; date of current version October 27, 2020. This work was supported in part by the National Natural Science Foundation of China under Grant 41575037, in part by the National Key Research and Development Plan of China under Grant 2016YFE0201900-02, and in part by the National Grand Fundamental Research 973 Programs of China under Grant 2014CB441403. The work of Haonan Chen was supported by the California Department of Water Resources and the Physical Sciences Division of NOAA Earth System Research Laboratory. *(Corresponding authors: Hui Xiao; Huiling Yang.)*

Yue Sun, Hui Xiao, and Li Luo are with the Key Laboratory of Cloud-Precipitation Physics and Severe Storms (LACS), Chinese Academy of Sciences, Beijing 100029, China, also with the Center of Disaster Reduction (CDR), Institute of Atmospheric Physics, Chinese Academy of Sciences, Beijing 100029, China, and also with the College of Earth and Planetary Sciences, University of Chinese Academy of Sciences (UCAS), Beijing 100049, China (e-mail: sunyue1@mail.iap.ac.cn; hxiao@mail.iap.ac.cn; luoli@mail.iap.ac.cn).

Huiling Yang and Liang Feng are with the Key Laboratory of Cloud-Precipitation Physics and Severe Storms (LACS), Chinese Academy of Sciences, Beijing 100029, China, and the Center of Disaster Reduction (CDR), Institute of Atmospheric Physics, Chinese Academy of Sciences, Beijing 100029, China (e-mail: yanghuiling@mail.iap.ac.cn; fengl@mail.iap.ac.cn).

Haonan Chen is with the Physical Sciences Division, NOAA/Earth System Research Laboratory, Boulder, CO 80305 USA, and also with the Cooperative Institute for Research in the Atmosphere, Fort Collins, CO 80523 USA (e-mail: haonan.chen@noaa.gov).

Color versions of one or more of the figures in this article are available online at http://ieeexplore.ieee.org.

Digital Object Identifier 10.1109/TGRS.2020.2982687

***Index Terms*— Inverse mapping table (IMT) method, polarimetric radar variables, raindrop size distribution (RSD), RSD parameter retrieval.**

I. Introduction

WEATHER radar is among the most important remote sensing detection equipment used to study cloud and precipitation processes [1]–[3]. Compared to the single-polarization radar methods, which only use reflectivity to retrieve rainfall intensity, the dual-polarization radar can obtain observations in both the horizontal and vertical polarization channels, which can provide more polarimetric variables [4], such as horizontal/vertical reflectivity (Z_H/Z_V), differential reflectivity (Z_{DR}), and specific differential propagating phase shift (K_{DP}). These polarimetric observables can better represent the microphysical characteristics of clouds and precipitation, making it physically possible to quantitatively retrieve the raindrop size distribution (RSD), which has become an important research topic over the past 20 years [5]–[15]. A gamma distribution is generally used to represent the RSD, which can depict the exponential distribution or single peak distribution in the domain $(0, +\infty)$. The gamma distribution has many equivalent forms [8], [16], [17]. The normalized gamma-type RSD [1] is commonly expressed in the following form:

$$N(D) = N_T \frac{(3.67+\mu)^{\mu+1}}{\Gamma(\mu+1) D_0} \left(\frac{D}{D_0}\right)^{\mu} e^{\left[-(3.67+\mu)\frac{D}{D_0}\right]} \quad (1)$$

where three independent parameters are included: total number concentration N_T (m^{-3}), median volume diameter (MVD) D_0 (mm), and shape parameter μ. The precise retrieval of RSD can not only improve the ability of dual-polarization radar in quantitative precipitation estimation (QPE) but also help to study the microphysical structure and precipitation process of clouds.

By using a scattering numerical model [18], [19], the theoretical values of different polarization variables can be calculated for a given set of hydrometeor types, shapes, and size distributions, as well as the radar wavelengths and environmental temperatures. However, it is challenging to represent those relationships using simple algebraic equations, since the change in the reflectivity and phase shift variables of raindrops may be nonlinear and even nonmonotonic [3] due to Mie scattering effects under the wavelength of weather radar. Therefore, many previous RSD retrieval algorithms have

attempted to establish the empirical or semiempirical relations between RSD parameters and polarimetric radar measurements. For example, the parameter β is introduced to treat the raindrop axis-ratio model as a variable [20], [21] and acts as an intermediate variable to help fit the semiempirical relations between polarimetric variables and RSD parameters [6], which is referred to as the beta method [8], [10]. Another common RSD retrieval method is the constrained-gamma (C-G) method [5], [7]. This method is mainly based on an empirical relationship between two RSD parameters built by ground observations from disdrometers, which can help to deduce and simplify the retrieving equations. The C-G method is found to be more applicable than the beta method in comparison studies based on the S-band [8] and X-band [10] radar measurements because the beta method is sensitive to the error in K_{DP}. The algorithm and skills to fit the nonlinear empirical relationship in the C-G method, such as the use of reflectivity-weighted mean diameter [11] and nearest-neighborhood method [15], can also affect the accuracy of the retrieval result. In addition to the abovementioned methods using explicit retrieving equations, there are also some improvements in the studies combining the probability methods. Cao *et al.* [22] proposed a Bayesian approach for retrieving the RSD parameters that produced better rainfall estimates compared to the previous empirical methods. Yoshikawa *et al*. proposed a maximum-likelihood algorithm to simultaneously deal with the attenuation and RSD parameter retrieval [13], and extended it to an X-band radar network by incorporating a Bayesian approach [14]. In [12], a 2-D variational approach is applied for multiple radars at different wavelengths.

Although these methods have proved to be effective under certain circumstances, most of them are based on an assumption on the shape parameter μ. For example, μ is assumed to be a constant in [13] and [14]. In addition, C-G empirical relationship exists in [12] and [22], which can be different for different precipitation types and/or regimes [8], [10], [23]. One limitation is that long-term observations may be necessary to build and assess those empirical relations for different types of precipitation once a radar is deployed at a new place. The conditional probability of related variables also needs to be obtained during the long-term observations. Another limitation is that when an empirical relationship based on ground observations is used to retrieve RSD parameters in the upper level above the ground, the relationship cannot always be verified, since the RSD measurements by aircraft are very limited. Theoretically, observations from multiple-wavelength radars may be a good solution since more information on consistencies and differences under different radar wavelengths can help to resolve the uncertainties. However, it is not always easy to build and deploy multifrequency radar systems.

To reduce the limitations of previous empirical methods in RSD retrieval, a physically based retrieval method, named the inverse mapping table (IMT) method, is proposed in this article. The IMT method is mainly based on the results of T-matrix scattering numerical simulation and does not depend on an empirical relationship with RSD parameters or polarimetric variables like the C-G method. The IMT method is also superior to the beta method which forms retrieval equations in a nonlinear product. The basic idea of the IMT method is to build an inverse mapping database directly by finding the intersection of two polarimetric variables in the coordinate system constructed by two RSD parameters, and then construct the monotonic relationship between the polarimetric variables and the third RSD parameter.

The remainder of this article is organized as follows. In Section II, the derivation and generation steps of the IMT method are introduced. In Section III, a convective rainfall case is selected to demonstrate the accuracy and efficacy in retrieving RSD parameters, and the C-G method [23] is also implemented for comparison, which includes noise sensitivity experiments and retrieval experiments under both ideal and real conditions. In Section IV, a large-scale rainfall case is selected to demonstrate the performances of the IMT in different types of rainfall. Section V discusses the error analysis and limitations of the IMT method. Section VI provides the summary and conclusion.

II. Inverse Mapping Table Method

A. Construction of the Forward Mapping Table From RSD Parameters to Polarization Variables

In the calculation of the T-matrix scattering numerical model [18], assuming certain orientations of raindrops, axis ratios of raindrop ellipsoid particles, and temperature-dependent dielectric parameters [24], the scattering characteristics can be computed. Although raindrops are hardly horizontal relative to the observed orientation of radar since there is usually nonzero elevation scanning, a number of approaches have been developed to perform elevation calibration [25]. Therefore, it is assumed that the raindrop is horizontal relative to the observed orientation of the radar. A model representing the empirical relationship between the axis ratio of a single raindrop ellipsoid particle and the equivalent spherical diameter established by Brandes *et al.* [9] has been widely applied in previous studies [7], [10], [12], [15]. In this article, a corrected version [26] of this model is applied

$$\mathrm{Ratio} = 0.9971 + 0.02193D - 0.035105D^2 + 0.0050746D^3 - 0.00023559D^4 \quad (2)$$

where Ratio is set to 1 when D is less than 0.5 mm. A scattering characteristic matrix database can be obtained such as Table I, which presents the scattering characteristics of a single raindrop. Based on the scattering characteristic matrix, the polarimetric radar variables are calculated as follows [1], [27]:

$$Z_{h,v} = \frac{4\lambda^4}{\pi^4 |K|^2} \int_{D_{\min}}^{D_{\max}} |f_{\mathrm{HH,VV}}(D)|^2 N(D)\, dD \quad (3)$$

$$Z_{\mathrm{DR}} = 10 \log_{10} \frac{Z_h}{Z_v} \quad (4)$$

$$K_{\mathrm{DP}} = \frac{180\lambda}{\pi} \int_{D_{\min}}^{D_{\max}} \mathrm{Re}\left[f_{\mathrm{HH}}(0, D) - f_{\mathrm{VV}}(0, D)\right] N(D)\, dD \quad (5)$$

$$\delta_{\mathrm{co}} = \arctan\left[\frac{\langle \overline{M}_{43} - \overline{M}_{34} \rangle}{\langle \overline{M}_{33} + \overline{M}_{44} \rangle}\right] \quad (6)$$

where D is the raindrop equivalent volume diameter; K_{DP} ($^\circ \cdot \mathrm{km}^{-1}$) is the specific differential phase; δ_{co} ($^\circ$) is

TABLE I
STRUCTURE OF THE DATABASE THAT CONSISTS OF SINGLE RAINDROP SCATTERING CHARACTERISTIC MATRIX

Level	I	Variables
Index / Variables	D: 0.1~10mm T:-20~35℃	Mueller matrix M amplitudes matrix f
Interval	D: 0.1mm, T: 5℃	
Size	100×12	

TABLE II
STRUCTURE OF THE FORWARD MAPPING TABLE

Level	I	Variables
Index/ Variables	T: -20~35℃ D_0: 0.1~4mm $\log_{10}(N_T)$: 1~6 (N_T: m^{-3}) μ: 0.9~16	Z_H, Z_{DR}, K_{DP}, δ_{co}...
Interval	T: 5℃, D: 0.1mm, $\log_{10}(N_T)$: 0.1, μ:0.1	
Size	12×40×51×170	

the backscatter differential phase; Z_h and $Z_v(\text{mm}^6 \cdot \text{m}^{-3})$ are horizontal and vertical reflectivity, respectively; λ is the radar wavelength; K is the dielectric factor of water; $f_{HH,VV}(D)$ are the backscattering amplitudes of a drop at horizontal and vertical polarization, respectively; $f_{HH,VV}(0, D)$ are the forward scattering amplitudes of a drop at horizontal and vertical polarization, respectively; Re(∗) stands for the real part of the complex number, and all M_{ij} values represent the components of the Mueller matrix; $D_{\min}$ is 0.1 mm as indicated in Table I, and $D_{\max}$ must be considered with the principle $D_{\max}/D_0 \geq 2.5$ [16], which helps to limit the error between the truncated summation and the total integral of a gamma-type RSD.

By enumerating three RSD parameters (μ, N_T, and D_0), the values of the polarization variables corresponding to those RSD parameters can be obtained through Table I, (1) and (3)–(6). Enumeration of the RSD parameters is applied to cover the ranges from previous studies [28], [29], and then, a database is obtained that maps the temperature and a set of three RSD parameters to the radar variables, which is called the forward mapping table (FMT; Table II). Here, the temperature of the raindrops is assumed as the atmospheric environmental temperature, which is determined by the sounding profiles from the nearest sounding stations or numerical weather model predictions. Then, it is necessary to determine whether there is only one set of RSD parameters corresponding to a given set of radar observations. If this inverse correspondence is unique, a database of inverse mapping can be constructed through this mapping relationship to determine the RSD parameters when radar observations are given.

B. Construction of an IMT From Two Polarization Variables to Two RSD Parameters

Considering the nonlinear forms of (3) and (4) and the nonmonotonicity of scattering characteristics, it is necessary to check whether there are multiple solutions on inverse mapping from radar measurements to RSD parameters. Nonlinear fitting on scatter plots is commonly used, but it is not easy to resolve unique mapping relations plotted between the variables when some overlapping points exist. In the IMT method, mutually mapping relationships between RSD parameters and polarimetric variables are established in analytical steps instead of through direct nonlinear fitting. It is first considered whether two RSD parameters and two radar polarization parameters can be mapped with each other when the other variables are fixed. The shape parameter μ in a gamma-type RSD is fixed as 0, which represents the common exponential distribution. The differences caused by temperature will be considered in Section II-E, by first assuming that the temperature is 20 °C. According to the FMT (see Table II), the distribution of Z_H and Z_{DR} in the (N_T, D_0) coordinate system can be obtained for fixed μ and temperature [see Fig. 1(a) and (b)]. Then, given a pair of Z_H and Z_{DR} values, the corresponding (N_T, D_0) pair should be the intersection of the contour line with the value of Z_H and the contour line with the value of Z_{DR}. Fig. 1(c) shows the determination of the intersection point when $Z_H = 30$ dBZ and $Z_{DR} = 2.5$ dB. The accuracy of the intersection position estimated in the above-mentioned method depends on the accuracy of the rectangular mesh in the original coordinates, and once the values of the four corners of the rectangular mesh are determined, the error of the intersection position estimation will not exceed the grid spacing of the original rectangular mesh. The technical details regarding how to obtain a contour figure and an intersection are briefly introduced in Appendixes A and B.

Therefore, to obtain corresponding (N_T, D_0) pairs, we only need to find the intersection point of the contour lines of the discrete Z_H and Z_{DR} values. According to the results calculated in Table II and the value range of polarization variables by observation, we take Z_H from 0 to 60 dBZ

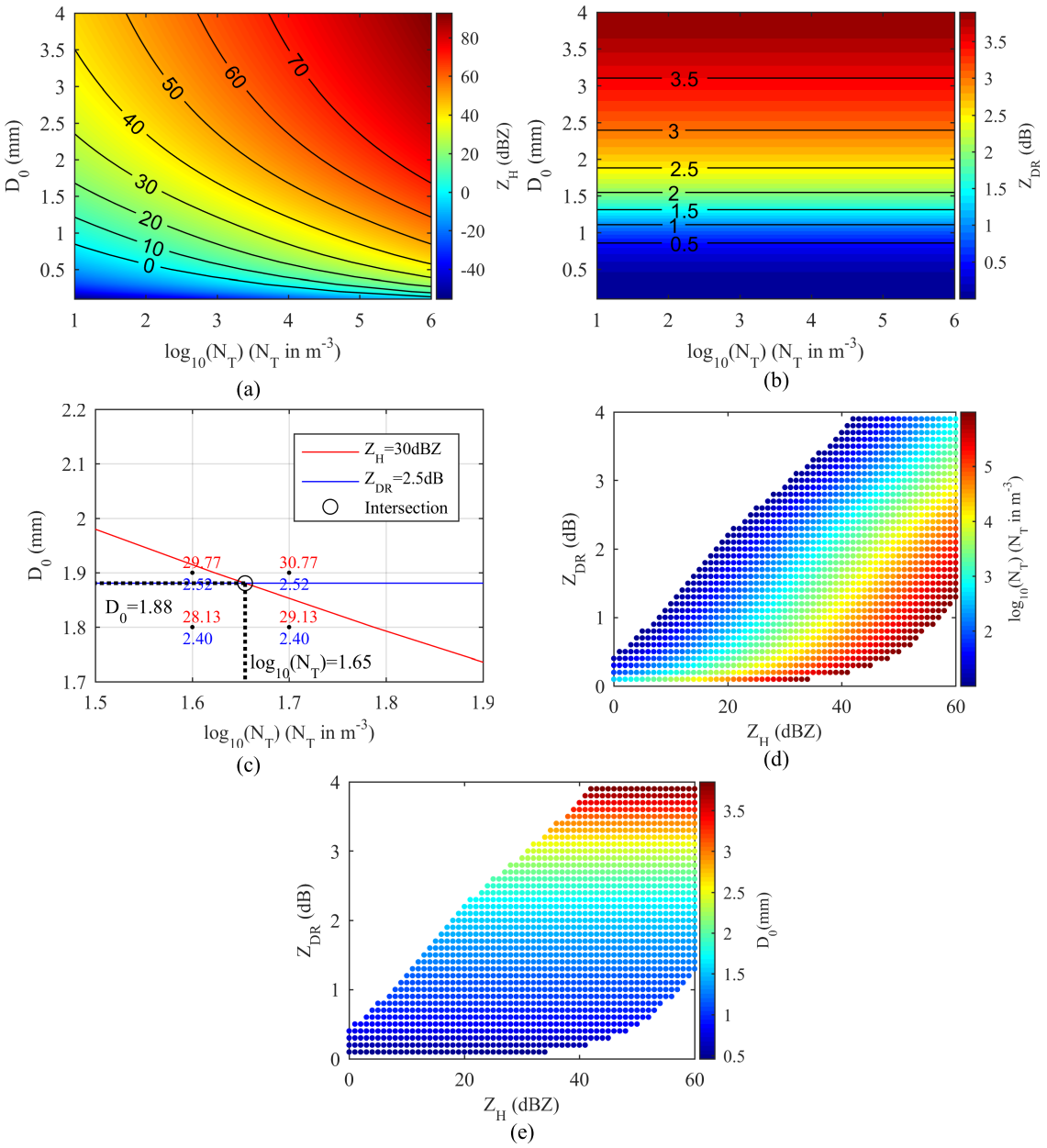

Fig. 1. Main steps of the construction of the reverse mapping table from Z_{H} and Z_{DR} to N_T and D_0: the distribution of (a) Z_{H} and (b) Z_{DR} in (N_T, D_0) coordinate system, (c) intersection position determined from the two contour lines of $Z_{\mathrm{H}} = 30$ dBZ and $Z_{\mathrm{DR}} = 2.5$ dB to get N_T and D_0 values, and (d) and (e) distributions of N_T and D_0 in (Z_{H}, Z_{DR}) coordinate system, respectively; the temperature is 20 °C and μ is fixed as 0.

with an interval of a certain value, e.g., 1 dB and Z_{DR} from 0 to 4.2 dB with a certain interval, e.g., 0.1 dB. Notably, the intervals of 1 and 0.1 dB for Z_{H} and Z_{DR}, respectively, are not representative of the actual accuracy of the radar. These parameters are usually the maximum sensitivities of weather radar, which is considered meaningful to distinguish. For example, the difference between $Z_{\mathrm{H}} = 30.11$ and 30.12 dBZ is not usually of concern, but a several-dB difference in Z_{H} may be of concern. By finding the intersection of the given (Z_{H}, Z_{DR}) pairs, all corresponding (N_T, D_0) pairs are retrieved. It is found that there is no result with more than one intersection showing the unique inverse mapping relationship on the domain of the RSD enumerated in Table II. Therefore, the distribution of N_T and D_0 on the (Z_{H}, Z_{DR}) coordinate system can be obtained [see Fig. 1(d) and (e)].

Although the distribution between Z_{H} and Z_{DR} in Fig. 1(e) seems redundant since D_0 can only be a function of Z_{DR} in previous methods (see [8]–[11]), there are still some benefits. One benefit is the consistency of the domains. When reasonable, finite, and clear ranges of D_0, N_T, and μ are set, there will be a regular 3-D domain for the RSD parameters, but the domain of the corresponding polarimetric variables is not regular. For example, there is no corresponding calculation result for $Z_{\mathrm{H}} = 10$ dBZ and $Z_{\mathrm{DR}} = 3$ dB, which means that a set of such polarimetric observations cannot retrieve the expected reasonable RSD parameters. However, in previous methods, it is not easy to prevent such inconsistency since the retrieving equations are often in the product form of variables. Another benefit is the method of recording a nonlinear relation between certain variables with limited error in each target

grid point, so it is not necessary to consider the details of nonlinear fitting, such as fitting form and sample point selection. Generally, once the results in Fig. 1(d) and (e) are obtained, the unique mutually mapping relationship between Fig. 1(d) and (e) and (a) and (b) can be determined. Thus, a single layer of the IMT from the two polarimetric radar parameters (Z_{H}, Z_{DR}) to the two RSD parameters (N_T, D_0) is established under a fixed μ condition.

C. Determination of the Three RSD Parameters Under Ideal Conditions

In Section II-B, we introduced a method to find the inverse mapping relation between polarimetric radar variables (Z_{H}, Z_{DR}) and RSD parameters (N_T, D_0) when μ is fixed. As long as μ is determined by other polarization variables of the radar, the single layer of IMT can be determined, and all three RSD parameters can be mapped in reverse. Therefore, another common polarimetric variable K_{DP} is considered first to help determine the RSD parameter μ.

A total of 170 values of μ from -0.9 to 16 with an interval of 0.1 are taken, and then, 170 layers of the IMT can be obtained by the inverse method presented in Section II-B. When the mutually mapping relationship between (N_T, D_0) and (Z_{H}, Z_{DR}) is obtained, the estimated value of K_{DP} at a given (Z_{H}, Z_{DR}) point can also be obtained, where the estimation error of K_{DP} is less than its variation between grids in the original rectangular cell. Then, for each point in the (Z_{H}, Z_{DR}) coordinate system, the μ-K_{DP} profiles can be obtained by combining the IMT layers corresponding to different discrete μ values whose maximum length of 170 is given in Table II according to 170 discrete μ values. The minimum length of the μ-K_{DP} profile is 0, where the (Z_{H}, Z_{DR}) pair does not match any RSD pair. The distribution of the length of these μ-K_{DP} profiles in the (Z_{H}, Z_{DR}) coordinate system is shown by the number of points in Fig. 2(a). These profiles in most regions have enough length to analyze the corresponding relationships between K_{DP} and μ, except for some regions at the upper left edge of the graph that corresponds to a small N_T. Some μ-K_{DP} profiles are shown in Fig. 2(b) as examples to illustrate the shapes of these profiles, which indicate that it is likely to vary monotonically. Thus, D_0 and N_T can be determined [see Fig. 2(c) and (d)] as long as μ is determined by K_{DP} according to the monotonicity at specific (Z_{H}, Z_{DR}) points. Now, it is only necessary to determine whether all μ-K_{DP} profiles vary monotonically, which can help to determine whether the only set of (N_T, D_0, μ) can be determined at a given set of Z_{H}, Z_{DR}, and K_{DP}. Here, to examine the monotonicity of the μ-K_{DP} profiles in all ranges, the statistic S to determine the monotonicity is designed as follows:

$$S = \frac{\sum_{i=1}^{n-1} \left(K_{\mathrm{DP}}\left(i+1\right) - K_{\mathrm{DP}}\left(i\right)\right)}{\sum_{i=1}^{n-1} \left|K_{\mathrm{DP}}\left(i+1\right) - K_{\mathrm{DP}}\left(i\right)\right|}. \tag{7}$$

The numerator of (7) is the sum of differences between adjacent values on the whole μ-K_{DP} profile and the denominator is the sum of absolute differences. Obviously, if the μ-K_{DP} profile is monotonically increasing, then S should be 1. If the profile is monotonically decreasing, then S should be -1. Therefore, if the profile is not monotonic, the value of S should be between -1 and 1. In particular, when increasing and decreasing segments have similar lengths or when there are large fluctuations in the profile, the value of S will be near zero. Fig. 2(e) shows the results of the monotonicity statistics. S is near -1 in most areas with a Z_{DR} larger than 2.4 dB [see Fig. 2(e)], indicating that the μ-K_{DP} relation has a monotonically decreasing trend. However, most areas smaller than 2.2 dB have the S values near 1, indicating that the μ-K_{DP} increases monotonically. The obvious changes in the monotonicity of the μ-K_{DP} profile only appears in a very narrow area of the Z_{DR} near 2.3 dB, and the S value near 0.5 dB of the Z_{DR} is approximately 0.5, indicating a partial increase in that area. Examples of μ-K_{DP} profiles with a poor monotonicity are given in Fig. 2(f), which indicates that a K_{DP} value does not correspond to a unique μ at specific (Z_{H}, Z_{DR}) points. However, the μ-K_{DP} varies monotonically in most regions, where a set of (Z_{H}, Z_{DR}, K_{DP}) does not correspond to a unique set of (N_T, D_0, μ). For the remaining areas where a set of (Z_{H}, Z_{DR}, K_{DP}) responds to one set of RSD parameters, the longest monotonic variation ranges of the μ-K_{DP} profiles are reserved. Then, a given K_{DP} value can be compared with each point on the monotonic μ-K_{DP} profile to find the nearest point to determine the μ value; thus, D_0 and N_T values can also be determined.

Although the above analysis gives the method using the polarimetric radar variable K_{DP} to determine the RSD parameter μ under ideal conditions, the accuracy of K_{DP} must be considered. Fig. 2(g) shows the range of K_{DP} changes in each profile. The range of K_{DP} varying with μ from -0.9 to 16 is less than 10^{-2} ($^\circ \cdot \mathrm{km}^{-1}$) when Z_{H} is less than 40 dBZ. Fig. 2(h) indicates that the magnitude of K_{DP} is less than 10^{-1} (°/km) when Z_{H} is less than 30 dBZ. It is difficult to ensure that the radar observations always have a higher precision than above such levels mentioned earlier. The error magnitude of K_{DP} estimated in each μ layer may be greater than the change of K_{DP} varying with μ, which indicates that the above-mentioned algorithm may not work very well in the case of weak reflectivity or rough quality control.

Another polarimetric radar variable is δ_{co} that refers to the differential phase. Although δ_{co} is not a variable directly observed by the polarimetric radar, it can be separated from observations by the difference between an FIR low-pass filter and an iteration filter according to previous studies (see [30]). Therefore, we can consider it as a direct variable that can be calculated by radar data. Through the same test (see Fig. 3), it is found that there are also monotonic characteristics in the μ-δ_{co} profiles [see Fig. 3(b)]. Most variation ranges are more than 10^{-1} (°) [see Fig. 3(c)], and most of the magnitude is larger than 10^{0} (°) [see Fig. 3(d)], which is partially greater than that in μ-K_{DP}. The areas with the S values near 0 also do not overlap with those in μ-K_{DP} profiles [see Fig. 3(a)]. Therefore, a set of (Z_{H}, Z_{DR}, δ_{co}) can also be used to retrieve (N_T, D_0, μ), and the μ-δ_{co} relationship is used to help determine μ in the area where μ-K_{DP} profiles have less monotonicity or change in magnitude.

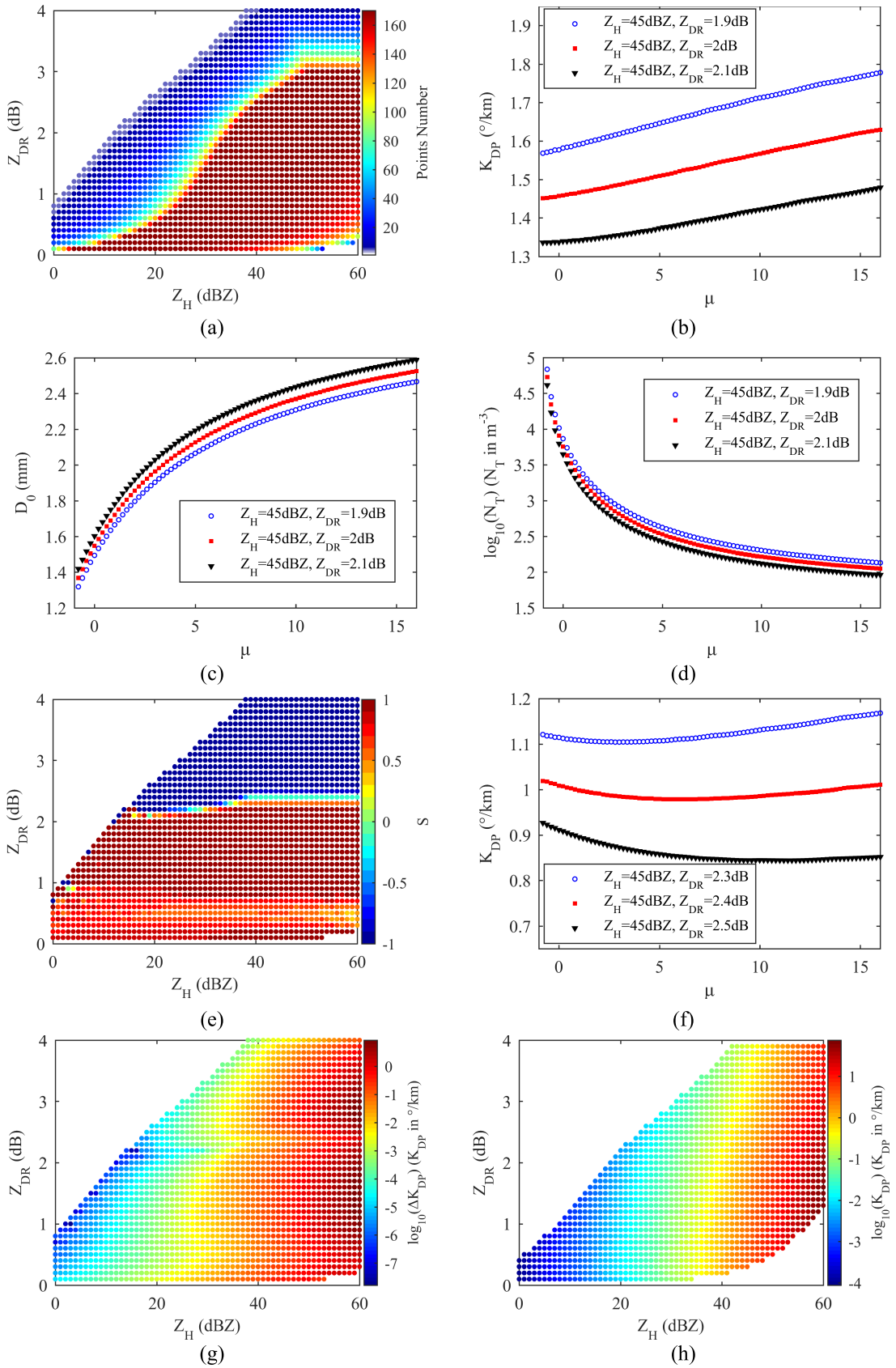

Fig. 2. Analyses of K_{DP} and μ in (Z_H, Z_{DR}) coordinate system. (a) Length of the μ-K_{DP} profiles at each point of 170 layers of μ from -0.9 to 16 with an interval of 0.1. (b) Examples of μ-K_{DP} profiles with high monotonicity. (c) Examples of the relationship between D_0 and μ at specific (Z_H, Z_{DR}) points. (d) Examples of the relationship between $\log_{10}(N_T)$ and μ at specific (Z_H, Z_{DR}) points. (e) Monotonicity test statistic S of μ-K_{DP} profiles. (f) Examples of μ-K_{DP} profiles with poor monotonicity. (g) Difference between the maximum and minimum K_{DP} values in each profile. (h) Distribution of K_{DP} at the layer of $\mu = 0$.

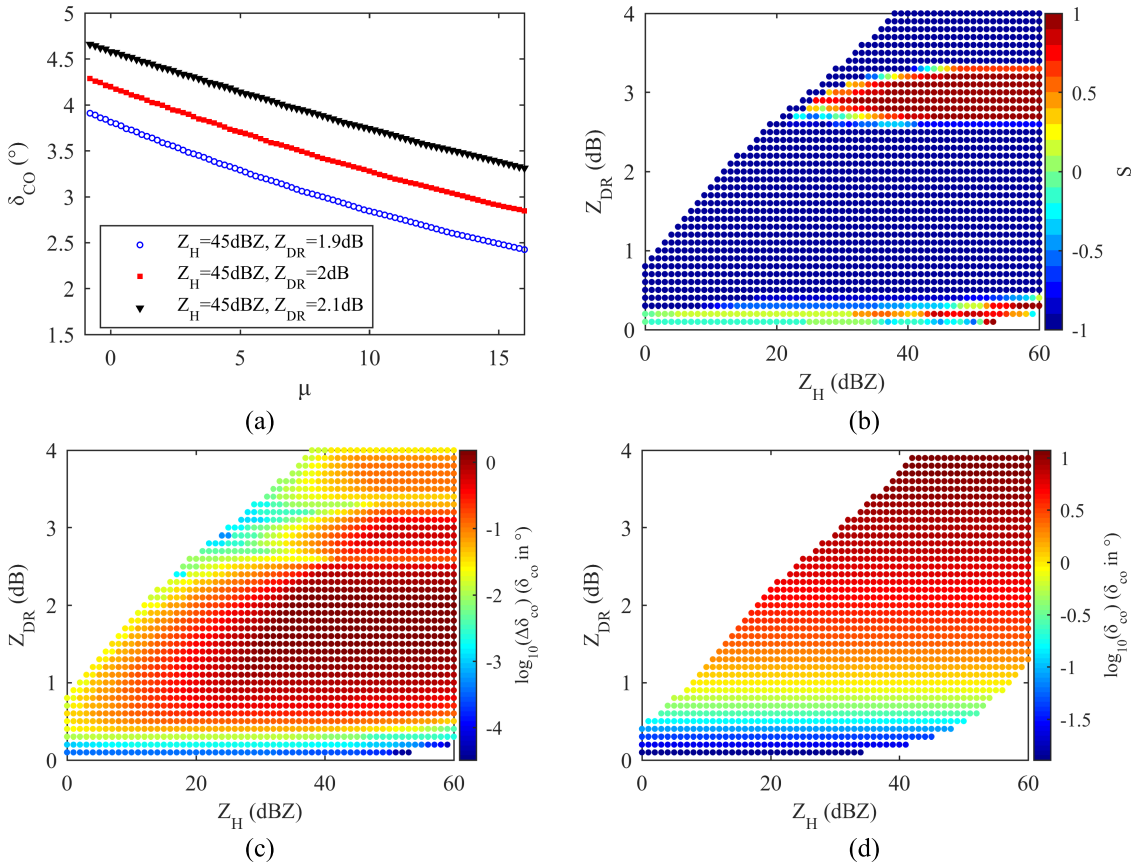

Fig. 3. Analyses of δ_{co} and μ in (Z_H, Z_{DR}) coordinate system. (a) Examples of μ-δ_{co} profiles. (b) Monotonicity test statistic S of μ-δ_{co} profiles. (c) Difference between the maximum and minimum δ_{co} values in each profile. (d) Distribution of δ_{co} at the layer of $\mu = 0$.

D. Determination of the Three RSD Parameters Under Real Conditions

The algorithm described in Section II-C is used to retrieve (N_T, D_0, μ) under ideal conditions, assuming that absolutely accurate K_{DP} and δ_{co} values can be obtained by radar observation and data quality control. However, this is difficult in real conditions. For example, when the rainfall intensity is not very severe, the variance in the differential phase (Φ_{DP}) may be smaller than the variance of noise, so filtering can only restrain the noise fluctuation to the greatest extent but cannot accurately restore the subtle changes in Φ_{DP} itself to reconstruct K_{DP} with high precision. Most methods for a quality control of Φ_{DP} and a reconstruction of K_{DP} can only provide a precision of approximately 0.1°/km [31]. Moreover, the separation of δ_{co} from an observed differential phase highly depends on the difference between the two filtering results, which also cannot guarantee that the results are always accurate. That is, absolutely accurate K_{DP} and δ_{co} are difficult to be retrieved under real conditions. Therefore, the synthetic differential phase shift effect, which can be expressed by K_{DP} and δ_{co}, is considered. ψ_{DP}^{obs} represents the differential propagation phase shifts directly observed by the radar, which is actually composed of four parts

$$\psi_{DP}^{obs} = \Phi_{DP} + \delta_{co} + \psi_0 + \text{noise} \tag{8}$$

where ψ_0 is the initial differential phase. Using an FIR low-pass filter [30], statistical fluctuation noise and sporadic ground clutter noise can be filtered out. Here, the remaining part is called the synthetic differential phase shift

$$K_{DP}^{FIR1} = \frac{1}{2}\frac{d\psi_{DP}^{FIR1}}{dr} = K_{DP} + \frac{1}{2}\frac{d\delta_{co}}{dr}. \tag{9}$$

Equation (9) is the sum of K_{DP} and the distance variation in δ_{co}. Since it is difficult to accurately separate them in practice, we will not separate them but directly discuss the corresponding relationship between (9) and the μ values. The first term K_{DP} on the right side of (9) can be calculated when a single layer of the reverse mapping table is constructed. The second term on the right side of (9) will be discussed as follows. Along the three dimensions (Z_H, Z_{DR}, μ) of the established inverse mapping database, the change of δ_{co} with distance r can be decomposed into three terms as follows:

$$\frac{d\delta_{co}}{dr} = \frac{\partial\delta_{co}}{\partial Z_H}\frac{dZ_H}{dr} + \frac{\partial\delta_{co}}{\partial Z_{DR}}\frac{dZ_{DR}}{dr} + \frac{\partial\delta_{co}}{\partial K_{DP}}\frac{dK_{DP}}{dr}. \tag{10}$$

The first term on the right side of (10) is 0 [see Fig. 3(d)] because when (Z_H, Z_{DR}, and μ) are determined, the change along the Z_H axis is only the number concentration, which is irrelevant to δ_{co}. As for the second term on the right side, $\partial\delta_{co}/\partial Z_{DR}$ can be obtained by a central difference using the established IMT dataset, and dZ_{DR}/dr can be obtained from the observed radial data. For the third term on the right side, $\partial\delta_{co}/\partial K_{DP}$ can also be obtained from the established IMT dataset since the dimension of μ can be replaced by K_{DP} according to the monotonicity of μ-K_{DP}. A challenge here is

TABLE III
STRUCTURE OF THE IMT

Level	I	II	III	Variables
Index / variables	T: -20~35°C	Z_H: 0~60dBZ Z_{DR}: 0~4.2dB	μ: -0.9~16	(N_T, D_0), K_{DP}, δ_{co} , $\partial\delta_{co}/\partial Z_{DR}$, $\partial\delta_{co}/\partial K_{DP}$
Interval	ΔT: 5°C	ΔZ_H: 1dBZ ΔZ_{DR}: 0.1dB	Δμ: 0.1	
Size	12	61 × 43	0~170	

to estimate the value of dK_{DP}/dr. It is the second derivative of Φ_{DP} along the radial direction, and the fluctuations of Φ_{DP} may produce high-order deviations in dK_{DP}/dr. Simple filtering techniques, such as median filtering, can also produce discontinuous curvature on Φ_{DP}, leading to an overestimation of dK_{DP}/dr. Therefore, the filtering processing should preserve the continuity and smoothness of Φ_{DP} before reconstructing K_{DP} and estimating dK_{DP}/dr. An example from real conditions will be given in Section III-A to show the operation and filtering result of Φ_{DP}. There are also some limitations of obtaining the available K_{DP} that will be discussed in Section V-C. As long as all the terms on the right side of (10) are obtained, the theoretical value of the synthetic differential phase shift effect in the IMT is presented as follows:

$$\left(\frac{1}{2}\frac{d\psi_{DP}}{dr}\right)^{Cal} = \left(\frac{\partial\delta_{co}}{\partial Z_{DR}}\right)^{Table}\frac{dZ_{DR}^{obs}}{dr} + \left(\frac{\partial\delta_{co}}{\partial K_{DP}}\right)^{Table}\frac{dK_{DP}^{FIR13}}{dr} + K_{DP}^{Table}. \quad (11)$$

In (11), superscript FIR13 represents 13 iterations of an iterative filtering to ensure noise suppression (referring to the maximum iteration times[30]), superscript Table stands for the data stored in advance in the IMT, and superscript obs symbolizes the calculation of polarization parameters from actual polarimetric radar observations. Thus, the value of the synthetic differential phase shift effect in (9) from the observations can be compared with the corresponding theoretical value in (11) at each fixed μ to help determine the μ value.

E. Extension of Inverse Mapping Table

Since the database of three RSD parameters inversely mapped by a set of polarimetric radar variables at different given temperatures has been established, one remaining task is to add the index by temperature in that database. The temperature index is taken from −20 °C to 35 °C at an interval of 5 °C, and a finer interval can be applied when necessary. Although raindrops that reached the ground rarely appear below 0 °C, the situation below 0 °C is still considered here in case of supercooled raindrops in the upper air above the freezing level. The database structure of the complete IMT is shown in Table III. This database takes up approximately 10^1–10^2 MB of computer memory in double precision, and its establishment processes only one time. Therefore, it does not need to be recalculated when retrieving RSD parameters. The process of retrieving RSD by the IMT method is shown in Fig. 4. Before starting the retrieval, the necessary quality control of the radar observation data is needed. Subsequently, the approximate location of the rainfall area can be judged by some hydrometeor classification algorithms, such as fuzzy logic [2], [3], or the warm water layer can be determined by temperature profiles from radiosonde or numerical forecasting.

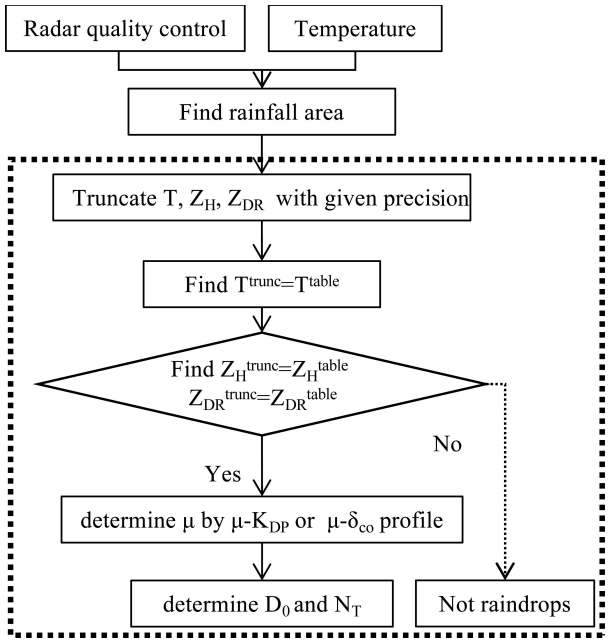

Fig. 4. Illustration of the IMT method to retrieve RSD parameters (the superscript trunc represents truncation with a specified precision.)

In addition, more factors can be included to the IMT, similar to the temperature information. For example, the observation elevation mentioned in Section II-A can be added as an index so that the elevation calibration process could possibly be omitted. Horizontal wind can also be treated as an independent index since wind speeds and directions can be retrieved given

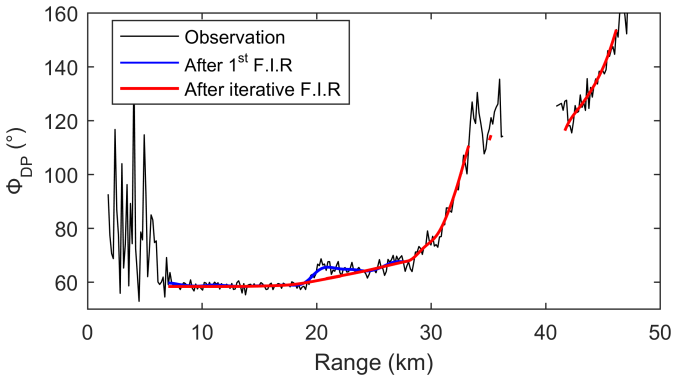

Fig. 5. Illustration of the Φ DP filtering. The radial profile is at 320° azimuthal angle from a 1.5° PPI scan at 10:28LST on July 13, 2011.

a Doppler radar network with sufficient overlap between the individual radar nodes. The empirical raindrop shape–size relation can also vary with different physical measurements, such as pressure and wind. Detailed quantification of the impacts induced by these factors will be investigated in a future study.

III. RSD Retrieval Experiment in a Convective Rainfall Event

A. Data

A squall line weather event that occurred in the Yitong area of Jilin Province in northeastern China on July 13, 2011, is selected as an example for retrieval verification first. The radar used in the observation is a 714XDP-A mobile X-band dual-polarization radar owned by the Key Laboratory of Cloud-Precipitation Physics and Severe Storms (LACS) of the Institute of Atmospheric Physics (IAP), Chinese Academy of Sciences (CAS) [32]. This radar was deployed at the Yitong observation site (125.50°E, 43.16°N), located 90 km south of Changchun, the capital city of Jilin Province in the summer of 2011 to develop observational experiments. An X-band weather radar often provides higher sensitivity than C-band and S-Band radars due to the higher frequency and plays an important role in precipitation monitoring and RSD retrieval [13], [14]. This kind of X-band radar also has advantages such as low cost and compact configuration due to the common size of its antenna compared to the other long-wavelength weather radars. However, a severe attenuation of X-band radar cannot be prevented when observing severe precipitation, so the quality control and attenuation correction always need to be considered. The performance and the basic method of data quality control and attenuation correction of this X-band radar can be seen in [32]. A modified iterative filtering is applied, and a sample result of filtering process is shown in Fig. 5. To reduce the effects of noise at the boundary layer near the radar and the large fluctuation near the edge of the cloud cells, the data along the radial range less than 8 km and near 40 km are masked according to the thresholds on the copolar correlation coefficients (CCs) and the standard deviation in Φ_{DP}. A lower threshold of 0.7 on copolar CCs and an upper threshold of 5° in the standard deviation in Φ_{DP} of 10 data range gates after deducting a linear trend are applied. Some data had a negative slope around 20 km after one FIR filtering, and these data are filtered after iterative filtering to prevent a bad K_{DP} with a negative value.

The selected RSD data are from a PARSIVEL^2 disdrometer [33] deployed by LACS at the observation site of the Yitong County Meteorological Bureau (125.28°E, 43.35°N, Station No.54164) in Jilin Province, China, and the disdrometer is located at 320.4° azimuth and 27.47-km distance of the radar and records the observed data of RSD every minute. For the basic quality control of RSD, Kruger and Krajewski's method was used [34], discarding the RSD observation data with a particle diameter larger than 8 mm or a gap larger than 60% compared to the empirical terminal velocity of raindrops proposed by Atlas *et al.* [35] as follows:

$$v(D) = 9.65 - 10.3 \cdot \exp(-6D) \tag{12}$$

where D(cm) is the equivalent diameter of a raindrop and v (m/s) is the terminal velocity of a raindrop with a diameter D. Then, the observed samples with rainfall intensity less than 0.1 mm/h or a particle number less than 10 are discarded. The parameters of RSD per minute are calculated by the third, fourth, and sixth moments of RSD observations [26], [36].

In this observation, the scanning mode of the radar has 1.5°, 2°, and 3° elevation angles of PPI scans first, and then several different azimuth angles are manually set to conduct RHI scanning in the high reflectivity area of those PPI scans. At the beginning of this local rainfall event, there was a mesoscale convective system that consisted of active convective cells [see Fig. 6(a) and (c)]; however, a severe convective line was formed later and passed over the location of the disdrometer [see Fig. 6(b)]. After 11:40 LST (local standard time, UTC +8), there were stratiform clouds with a bright band presented in the observed region [see Fig. 6(d)]. Considering the difference in sampling space between the radar and the disdrometer and the fluctuation in the radar data, the average values of 15 range gates around the disdrometer (three nearest azimuths and five nearest range gates at a specific azimuth in the 1.5° PPI) are compared with the polarization variables simulated by RSD [see Fig. 7(a)–(c)]. Although it is not easy to compare radar data with disdrometer observations precisely every minute due to the larger time interval of radar observation data and the rapid change in weather processes, the variation trend and magnitude of polarization variables are basically consistent between the observations of the polarimetric radar and the disdrometer, except that K_{DP} has a small order of magnitude in the later period of this precipitation event that occurred on July 13. The obvious rainfall process lasted from 10:15 to 12:48 LST [see Fig. 7(d)], and in the early stage it was mainly the obvious convective precipitation in the front of the squall line. The peak reflectivity after attenuation correction was close to 60 dBZ, and the peak rainfall intensity observed by the disdrometer was above 80 mm/h, but the peak duration was short. In the later stage, it was mainly the stratiform cloud precipitation behind the squall line. The total accumulated precipitation was 25.6 mm. The benefit of choosing a squall line case is that there is a high reflectivity and a severe convective rainfall in the front part of a squall line and low reflectivity and lighter rainfall in the stratiform cloud area at the back of the squall

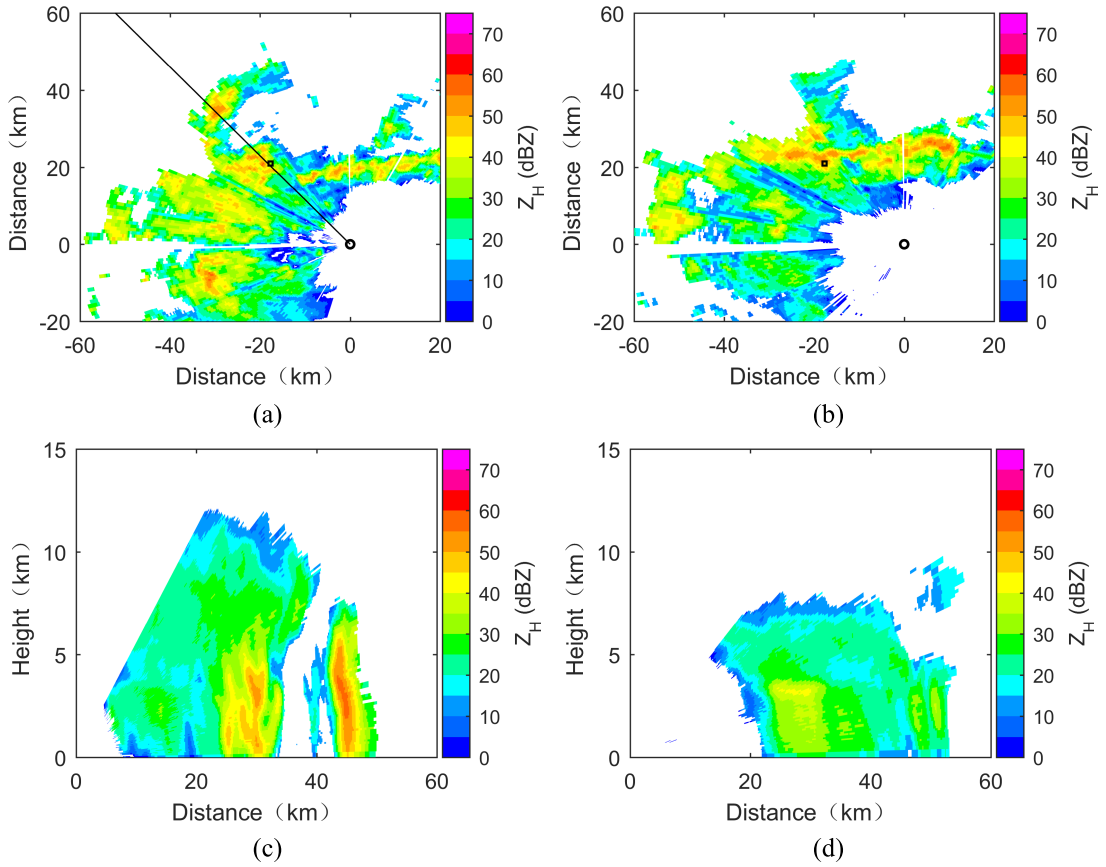

Fig. 6. Sample observations of Z_H (after quality control and attenuation correction) during the precipitation case on July 13, 2011. (a) 1.5° PPI at 10:21LST. (b) 1.5° PPI at 10:44LST. (c) 320° RHI at 10:21LST. (d) 320° RHI at 11:42 LST. The black circle and square in (a) and (b) are the locations of the radar and the disdrometer, respectively. The black line in (a) shows the same azimuthal direction as the RHI scans in (c) and (d).

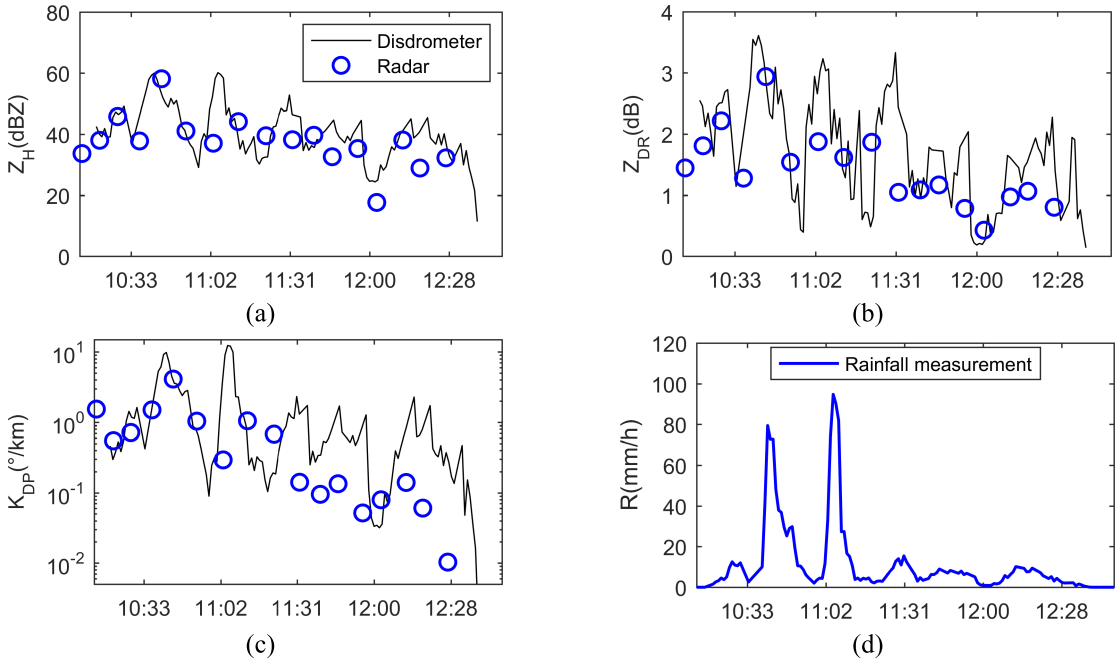

Fig. 7. Comparison between radar data (blue circles) after quality control and simulated radar data (black line) based on RSD parameters on July 13, 2011. (a) Z_H. (b) Z_{DR}. (c) K_{DP}. The radar PPI data at 1.5° elevation angle were used. The corresponding rainfall rates calculated from disdrometer data are indicated in (d).

line [see Fig. 7(a)–(d)]. Therefore, we can evaluate the retrieval method in different weather and precipitation conditions within one case.

B. C-G Method for Comparison

A comparable method for RSD parameters retrieval is necessary to examine whether the proposed IMT method

can improve the retrieval accuracy, efficiency, applicability, or provide other benefits. Li *et al.* [23] built RSD parameters retrieval equations based on the C-G method [10] in the same place and using the same radar and disdrometer mentioned in Section III-A. This C-G method is briefly introduced as follows.

The C-G relation fitted from several rainfall processes, including the convective rainfall event demonstrated in Section III-A, is shown as follows:

$$\mu = -0.0211\Lambda^2 + 1.365\Lambda - 1.575 \tag{13}$$

where $\Lambda(\mathrm{mm}^{-1})$ is the scale parameter of a gamma distribution and can be converted into the following theoretical relation:

$$\Lambda D_0 = \mu + 3.67. \tag{14}$$

The form of gamma-type RSD used in [23] is as follows:

$$N(D) = N_w \frac{6}{3.67^4} \frac{(3.67+\mu)^{\mu+4}}{\Gamma(\mu+4)} \left(\frac{D}{D_0}\right)^{\mu} e^{\left[-(3.67+\mu)\frac{D}{D_0}\right]} \tag{15}$$

where N_w is the intercept factor, which represents the intercept in the Y-axis when μ is equal to 0. The empirical relation between MVD D_0 (mm) and Z_{DR} (dB) is fitted after (13) is obtained when D_0 depends on Z_{DR}

$$D_0 = 0.65 + 0.79 Z_{\mathrm{DR}}. \tag{16}$$

Once D_0 is obtained, μ can be calculated by (13) and (14). The nonlinear semiempirical relation to calculate the water content W (g/m^3) is as follows:

$$W = 10^{-3} Z_h 10^{\left(-2.48 Z_{\mathrm{DR}} + 1.72 Z_{\mathrm{DR}}^2 - 0.5 Z_{\mathrm{DR}}^3 + 0.06 Z_{\mathrm{DR}}^4\right)} \tag{17}$$

where the unit of Z_h is $\mathrm{mm}^6 \cdot \mathrm{m}^{-3}$. The intercept factor N_w can be calculated after W and D_0 are obtained

$$N_W = 57526 \cdot W / D_0^4. \tag{18}$$

Then, the total number concentration N_T can be calculated by combining (1) and (15) once μ, D_0, and N_w are all obtained. Equations (1) and (13)–(18) form the C-G method, which will be applied in the following sections for comparison with the IMT method.

C. RSD Retrieval Under Ideal Conditions

There are still some challenges in evaluating the RSD parameter retrieval method by comparing with the disdrometer observations. First, deviations can be introduced by the differences of sampling times and spaces between the radar and the disdrometer. A radar observation represents the instantaneous state of weather targets above the ground, while a disdrometer observation is the short-term accumulation of raindrops on the ground, which can be influenced by wind, especially during the convective event. Second, the performance of the disdrometer limits the accuracy of recording RSD [37]–[39]. The PARSIVEL^2 disdrometer used in this article may produce an overestimation of large drops and an underestimation of small drops under some heavy rainfall conditions [40]. Additionally, data processing, such as estimation of RSD parameters by the disdrometer data and the radar data after quality control, can also introduce some uncertainty. All these factors mentioned above may disturb either the evaluations of the retrieval method or the comparison of the method with other different methods. Therefore, retrieval experiments under ideal conditions are necessary. The "ideal" radar observations are simulated according to RSD parameters retrieved from the disdrometer, under the assumption that the polarization variables observed by the radar are consistent with the disdrometer to prevent any noise or disturbance factors.

According to the retrieving method under the ideal conditions discussed in Section II-C, three parameters (N_T, D_0, μ) in (1) will be retrieved as the result of the IMT method, as well as the other two variables, rain water content W (19), (g/m^3) and rainfall intensity R (20), (mm/h), which are of concern in numerical weather models or practical applications of clouds and precipitation studies

$$W = \frac{\pi \rho_w}{6} \sum N(D_i) \cdot D_i^3 \cdot \Delta D \tag{19}$$

$$R = \frac{\pi}{6} \sum N(D_i) \cdot D_i^3 \cdot v(D_i) \cdot \Delta D \tag{20}$$

where ρ_w is the density of water, and v is the terminal velocity referred to that in (12). The retrieval results using the C-G method are calculated according to Section III-B and (20).

The retrieval results are shown in Fig. 8. For D_0, the two methods have similar retrieving abilities [see Fig. 8(a)]. For μ, although it seems not completely accurate and there are some differences between the IMT and C-G methods, both methods produced trends and the locations of peaks that are consistent with the referenced observations [see Fig. 8(b)], which indicate that the IMT method has a certain ability to retrieve μ without using empirical relations. For $\log_{10}(N_T)$, although the trends are roughly retrieved by both methods, there are some points that produced deviations of a larger order of magnitude [see Fig. 8(c)]. However, as for the results of W and R, there are obvious differences between the two methods. Before 11:00 LST, the results of the C-G method are approximately one to two orders of magnitude larger than the expected results, while the IMT results remain better in the whole process. It is not easy to completely explain such an error in the C-G method, but one reasonable guess is that the input values of Z_{H} and Z_{DR} exceeded the expected domain in (17) and (18), and then, the error was produced by nonlinear extrapolating effects in (17) and (18). These kinds of deviations will be briefly discussed in Section V-B.

To further quantitatively evaluate the retrieval accuracy, the following common statistics are given: mean absolute error (MAE) (21), mean relative error (MRE) (22), and CC (23):

$$\mathrm{MAE} = \frac{\sum_{i=1}^{n} |q_i^{\mathrm{calc}} - q_i^{\mathrm{obs}}|}{n} \tag{21}$$

$$\mathrm{MRE} = 100 \cdot \frac{\sum_{i=1}^{n} \left(\frac{q_i^{\mathrm{calc}} - q_i^{\mathrm{obs}}}{q_i^{\mathrm{obs}}}\right)}{n} \tag{22}$$

$$\mathrm{CC} = \frac{\sum_{i=1}^{n} \left(q_i^{\mathrm{calc}} - \overline{q^{\mathrm{calc}}}\right)\left(q_i^{\mathrm{obs}} - \overline{q^{\mathrm{obs}}}\right)}{\sqrt{\sum_{i=1}^{n} \left(q_i^{\mathrm{calc}} - \overline{q^{\mathrm{calc}}}\right)^2 \cdot \sum_{i=1}^{n} \left(q_i^{\mathrm{obs}} - \overline{q^{\mathrm{obs}}}\right)^2}} \tag{23}$$

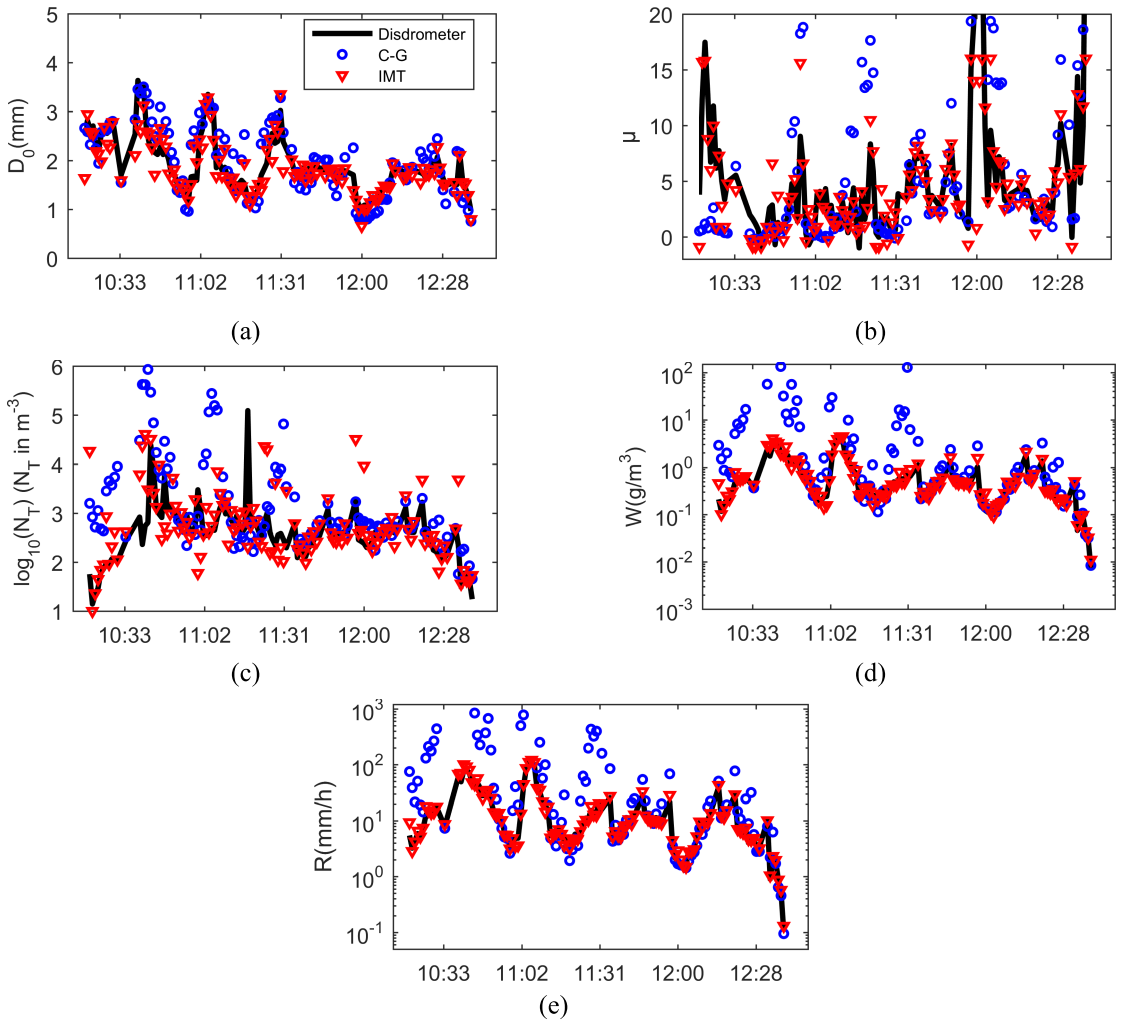

Fig. 8. Comparison of the three RSD parameters, water content, and rainfall intensity between the observations and the results retrieved by the C-G and the IMT methods under ideal conditions on July 13, 2011. (a) D_0 (mm). (b) μ. (c) $\log_{10}(N_T)$ (N_T in m^{-3}). (d) Water content W (g/m^3). (e) Rainfall intensity R (mm/h). W and R are simulated by the three RSD parameters fit from disdrometer data with terminal velocity model in (12).

TABLE IV

RETRIEVAL ACCURACY DURING A CONVECTIVE RAINFALL EVENT BY THE IMT METHOD AND C-G METHOD UNDER IDEAL CONDITIONS

Methods		D_0 (mm)	μ	$\log_{10}(N_T)$ (N_T in m^{-3})	W(g/m^3)	R(mm/h)
IMT	MAE	0.16	1.84	0.38	0.12	1.83
	MRE (%)	-2.17	17.18	6.48	7.30	4.11
	CC	0.91	0.77	0.50	0.98	0.99
C-G	MAE	0.28	3.41	0.66	48.28	1312.58
	MRE (%)	4.23	-38.51	23.51	2158.14	2138.54
	CC	0.88	0.66	0.34	0.61	0.64

In (21)–(23), q is the variable to be evaluated, superscript calc represents the retrieval results, and superscript obs represents the results measured by disdrometer. MAE and MRE are used to present the magnitude of the overall proportion in the MAE and the MRE of retrieval, respectively, and CC is used to reflect the consistency of fluctuations and trends between the observations and retrieval results. Noting the retrieval accuracy of the IMT method and the C-G method for the whole precipitation event (see Table IV), the IMT method produced better results in all the statistical indicators, while the C-G method failed to retrieve W and R. Moreover, the precipitation event is roughly divided into a convective rainfall period (10:15–11:40 LST) and a stratiform rainfall period (11:41–12:48 LST) according to the macrostructure of reflectivity depiction [see Fig. 6(c) and (d)] used to obtain comparisons. The C-G method produced worse results than the

TABLE V
SAME AS TABLE IV, BUT ONLY FOR THE CONVECTIVE RAINFALL PERIOD (10:15–11:40 LST)

Methods		D_0 (mm)	μ	$\log_{10}(N_T)$ (N_T in m^{-3})	W(g/m^3)	R(mm/h)
IMT	MAE	0.22	1.51	0.48	0.16	2.54
	MRE (%)	-2.09	7.53	7.50	6.56	3.58
	CC	0.88	0.86	0.39	0.98	0.99
C-G	MAE	0.32	3.39	0.95	80.98	2201.79
	MRE (%)	9.46	-34.9	33.28	3595.69	3562.51
	CC	0.86	0.33	0.21	0.61	0.64

TABLE VI
SAME AS TABLE IV BUT ONLY FOR THE STRATIFORM RAINFALL PERIOD (11:41–12:48 LST)

Methods		D_0 (mm)	μ	$\log_{10}(N_T)$ (N_T in m^{-3})	W(g/m^3)	R(mm/h)
IMT	MAE	0.09	2.32	0.23	0.06	0.78
	MRE (%)	-2.30	31.35	4.99	8.39	4.89
	CC	0.94	0.72	0.75	0.98	0.99
C-G	MAE	0.22	3.43	0.24	0.24	6.00
	MRE (%)	-3.46	-43.83	8.27	47.32	46.18
	CC	0.89	0.77	0.78	0.88	0.86

IMT method in the convective rainfall period (see Table V) and more similar deviation levels in the stratiform rainfall period (see Table VI), which indicated the basic capability and better applicability of the IMT method for RSD parameters retrieval compared with the previous method.

D. Noise Sensitivity Experiments

The impacts of noise on retrieving RSD parameters by using radar data often need to be assessed. Besides the system noise of the radar, there are also some factors that cause measurement noise. For example, there are often violent changes of the wind field in a convective system since severe updraft, downdraft, and divergence exist and may change rapidly, which can distort the orientation of the raindrops and make the raindrops oscillated. Under those conditions, the measurement of differential phase shift and differential reflectivity will be contaminated since they are sensitive to the orientations of the observed targets, thus, the noise sensitivity of a method based on these variables needs to be considered.

One difficult issue in examining the noise sensitivity of the IMT method is that all relations for retrieving RSD parameters are organized in the inverse mapping database instead of some equations. Therefore, the retrieval errors/deviations caused by noise are only in database form, which makes it difficult to evaluate the noise sensitivity by adding noise terms and deducing equations to obtain a noise sensitivity function [8]. However, random noise experiments may help to compare the noise sensitivity between the IMT and C-G methods. The noise in the reflectivity is first considered. Based on the ideal values of Z_H (dBZ) and Z_{DR} (dB) in Section III-A, Z_V is calculated by Z_H–Z_{DR} relations. Two series of Gaussian random numbers with a certain standard deviation (σ) are generated each time to be added to Z_H and Z_V. Therefore, the time series of Z_H and Z_{DR} with random noise of a certain magnitude can be obtained each time. By assuming that σ varies from 0 dB to 6 dB with an interval of 0.1 dB and repeats 30 times with a specific σ, the comparison of sensitivity to noise in reflectivity between the C-G method and the IMT method can be obtained (see Fig. 9). Although under the condition that the noise σ is lower than 1 dB, the error increases faster in the IMT method, the differences in D_0 are fairly small, and the differences in $\log_{10}(N_T)$ are no more than one order of magnitude. However, when σ is larger than 1 dB, the D_0 error in the C-G method increases linearly, which can be expected in (16), while the D_0 error in the IMT method increases slowly and the MAE is near 1 mm [see Fig. 9(a)]. For $\log_{10}(N_T)$, the errors grow rapidly from 4 to 8 in MAE of $\log_{10}(N_T)$ in the C-G method, which seems worthless in relevant research and application, while errors grow slower and not more than 2 MAE in $\log_{10}(N_T)$ when the IMT method is used [see Fig. 9(b)]. These differences can be considered from two aspects. First, the MAE growth in the IMT method under small noise may be caused by the truncation of Z_H and Z_{DR}, which can produce a value jump in the input variables. These errors grow slowly with the magnitude of noise since there is no linear or nonlinear multiplication. The noise may produce a deviation in the mapping database but not like that in the C-G method, where some variables are multiplied together. In addition, the consistency of the domains mentioned in Section II-B may help to prevent extrapolation conditions. However, the two methods show similar noise sensitivity when retrieving μ.

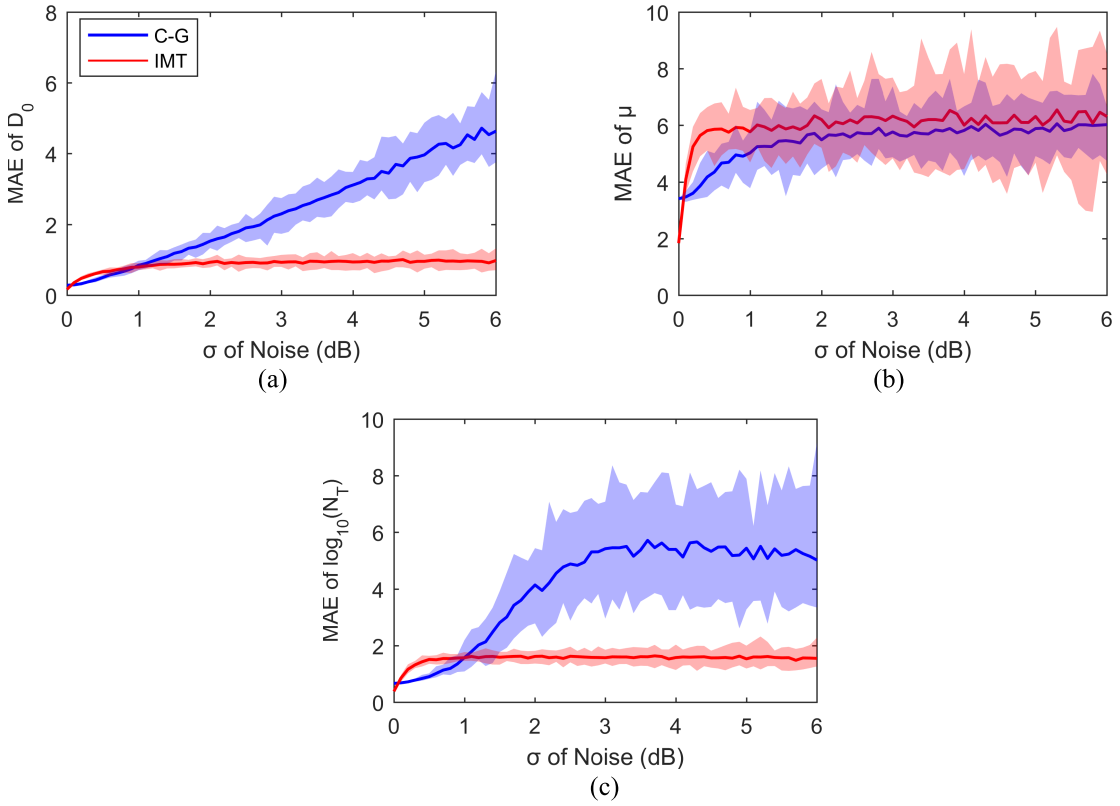

Fig. 9. Comparison of sensitivity to noise in reflectivity between C-G and IMT methods. (a) MAE of D_0 (mm). (b) MAE of μ. (c) MAE of $\log_{10}(N_T)$ (N_T in m^{-3}). Solid colored lines are the average of 30 random noise experiments each with different standard deviation σ of Gauss distribution noise, and the shaded regions represent the MAE ranges of the random experiments.

Although the IMT method shows a better performance than the C-G method in terms of sensitivity to noise in reflectivity, the C-G method does not depend on differential phase variables. That is, if the IMT method is extremely sensitive to the noise in K_{DP} and δ_{co}, its applicability is still limited. Therefore, similar random noise experiments are designed. Two series of random noise act as a relative error added to both K_{DP} and δ_{co}, and σ varies from 10% to 1000% with an interval of $\log_{10}(0.1)$. The results show that the IMT method is not more sensitive to noise in differential phase variables than it is to reflectivity. Even a 1000% relative error noise only produces a 0.6 mm MAE for D_0 [see Fig. 10(a)]. The MAE of μ reached 6 under 100% relative error noise [see Fig. 10(b)], which is similar to the sensitivity to noise in reflectivity [see Fig. 9(b)]. The MAE of $\log_{10}(N_T)$ is also limited. Though these random experiments do not represent all conditions, a lower sensitivity to noise has been shown in the IMT method than in the previous C-G method.

E. RSD Retrieval Under Real Condition

Although the accuracy of the IMT method in retrieving RSD parameters in Section III-C has been verified under ideal conditions, it is mainly based on the assumption that K_{DP} and δ_{co} can be accurately separated from the original observations after data quality control. Under real conditions in the radar observations and operations, the IMT method should be evaluated using a similar scheme based on the synthetic differential phase shift effect proposed in Section II-D to test its reliability in practical applications. Fig. 11 shows the comparison between the retrieval results of the IMT method and the C-G method using actual radar observations. The retrieval results are averaged in the same way as those in Fig. 7, which are the average results of 15 range gates. The error analysis, as shown in Table IV, is not presented since the sampling time and space of the radar and disdrometer cannot always be sufficiently consistent and comparable in such severe convective weather. However, similar results can be found in Fig. 11 compared with the ideal condition in Fig. 8. For example, the retrieved D_0 values are similar in the two methods. The μ values retrieved from the two methods are partially consistent with the expected values. There are still larger errors in the water content W and rainfall intensity R when the C-G method is used, especially for rainfall intensities near 10^3 mm/h in the early stage of the rainfall event, which are obviously unreasonable. Compared with that value, the values of W and R retrieved by the IMT method are more reasonable, indicating a better applicability of the new method in this convective rainfall case.

IV. RSD Retrieval Experiment in a Large-Scale Rainfall Event

A large-scale rainfall process that occurred in the same region from 19:12 LST August 15 to 4:48LST August 16, 2011 is selected to assess whether the IMT method still has a better performance in a different rainfall type. The variation trend and magnitude of polarization variables are basically consistent between the observations of the dual-

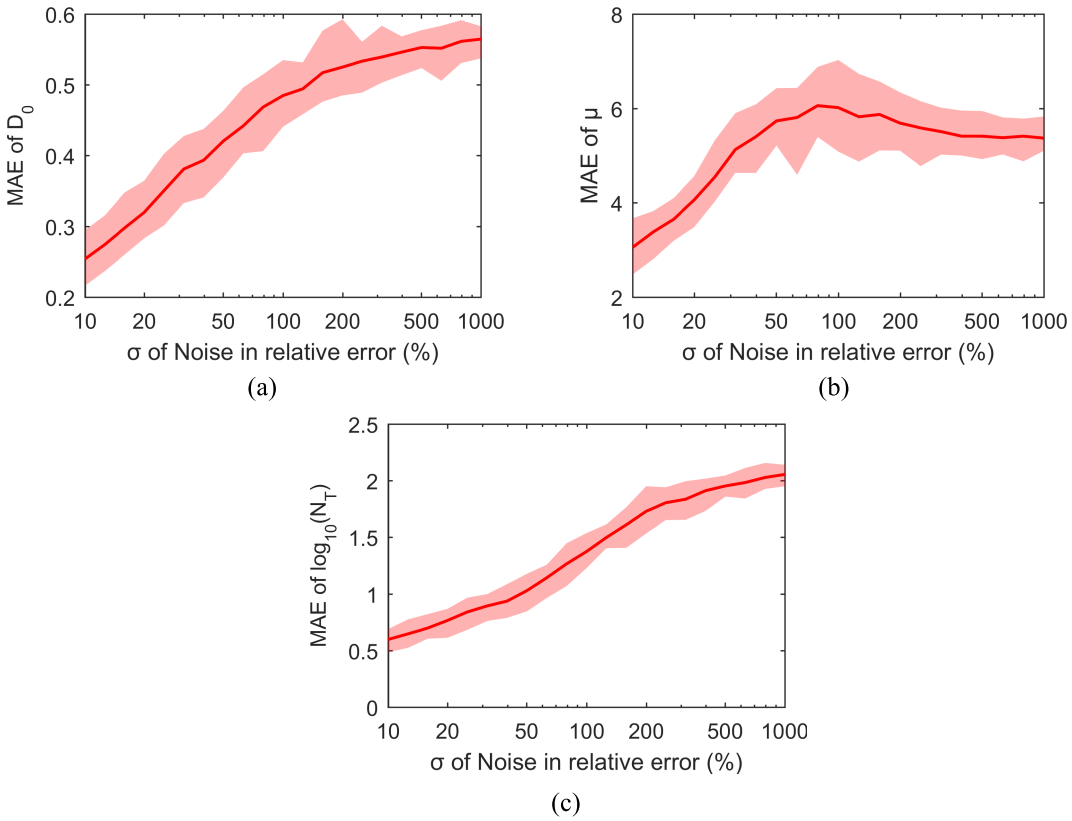

Fig. 10. Sensitivity to noise represented by a relative error (σ) both in K_{DP} and δ_{co} when using the IMT method: (a) MAE of D_0 (mm); (b) MAE of μ; and (c) MAE of $\log_{10}(N_T)$ (N_T in m^{-3}). Solid colored lines are the average of 30 random noise experiments each with different standard deviation σ of Gauss distribution noise, and the shaded regions represent the MAE ranges of the random experiments.

TABLE VII

RETRIEVAL ACCURACY DURING A LARGE-SCALE RAINFALL EVENT BY THE IMT METHOD AND THE C-G METHOD UNDER REAL CONDITIONS

Methods		D_0 (mm)	μ	$\log_{10}(N_T)$ (N_T in m^{-3})	W(g/m^3)	R(mm/h)
IMT	MAE	0.13	6.03	0.37	0.27	3.21
	MRE (%)	-2.54	-37.64	6.94	40.63	74.4
	CC	0.61	0.004	0.24	0.43	0.57
C-G	MAE	0.17	7.9	0.64	0.34	3.60
	MRE (%)	-5.76	130.18	-15.78	-47.58	-42.88
	CC	0.50	0.37	0.07	0.31	0.56

polarization radar and the disdrometer [see Fig. 12(a)–(c)], even though there are some frames with underestimated K_{DP} [see Fig. 12(c)]. The local rainfall lasted for about 10 h [see Fig. 12(d)] with a mean value about 4.1 mm/h in the first half and 1.2 mm/h in the second half. Since the radar data are from continuous volume scans and the rainfall event is more stable than the convective case in Section III, the retrieval experiment under ideal conditions is omitted and the retrieval results under real conditions are shown (see Fig. 13). The retrieval result at every radar data time (9-min interval according to the volume scans) is compared with the disdrometer data at adjacent time to obtain the retrieval error statistics (see Table VII). The two methods have similar error level in retrieving D_0, $\log_{10}(N_T)$ and W for this continuous weak rainfall process, and the IMT method produces slightly better MAE, MRE, and CC in these variables. The error level of the IMT method in retrieving R is a little lower in MAE and CC, but essentially similar to the C-G method. However, the IMT method fails to retrieve the variation trends of μ [see Fig. 13(b)] since the CC is near zero. One possible reason for the deviation is the differences between small raindrops on the ground and above the ground, since the small raindrops falling slowly may evaporate before they reach the ground so that the shape of RSD may be different. Overall, the results indicate that the IMT approach still has a good performance to retrieve most related parameters during this large-scale rainfall case.

V. DISCUSSION

A. Error Analysis of the IMT Method

From the retrieval results under the ideal conditions shown in Section III-C, there are still some offsets at times when the retrieval results deviate greatly from the reference observation values, which mean that the "inverse mapping" is

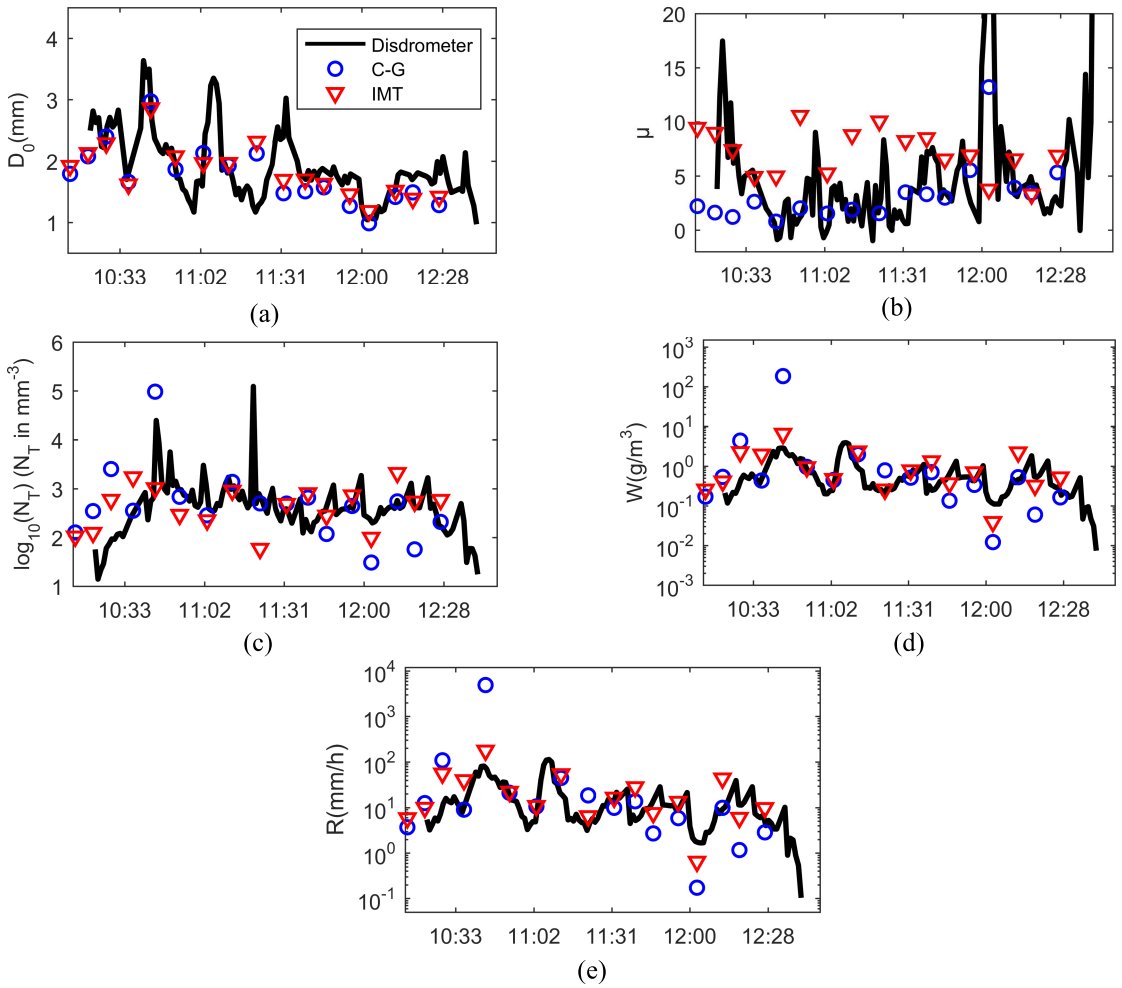

Fig. 11. Comparison of the three RSD parameters, water content and rainfall intensity between the observations and the results retrieved by the C-G and the IMT methods under real conditions on July 13, 2011: (a) D_0 (mm); (b) μ; (c) $\log_{10}(N_T)$ (N_T in m^{-3}); (d) water content W (g/m^3); and (e) rainfall intensity R (mm/h).

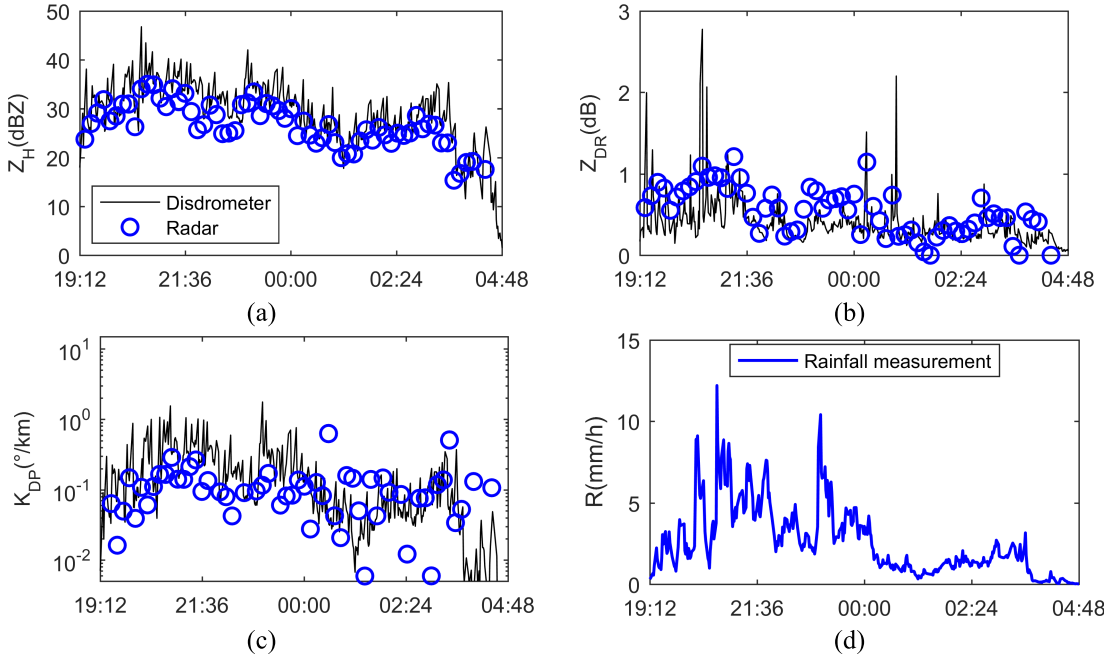

Fig. 12. Comparison between radar data (blue circles) after quality control and simulated radar data (black line) based on RSD parameters in the large-scale rainfall event from 19:12 LST August 15 to 4:48 LST August 16, 2011. The radar PPI data at 0.5° elevation angle were used.

not accurately realized all the time. To address this, the errors of μ and $\log_{10}(N_T)$ at each time point are analyzed and found to be related to the value of Z_{DR} (see Fig. 14). The points with a large error of μ are concentrated in the areas below 0.3 dB and near 2.5 dB of Z_{DR}, where the monotonicity of μ-δ_{co} and μ-K_{DP} relationships are relatively poor [see

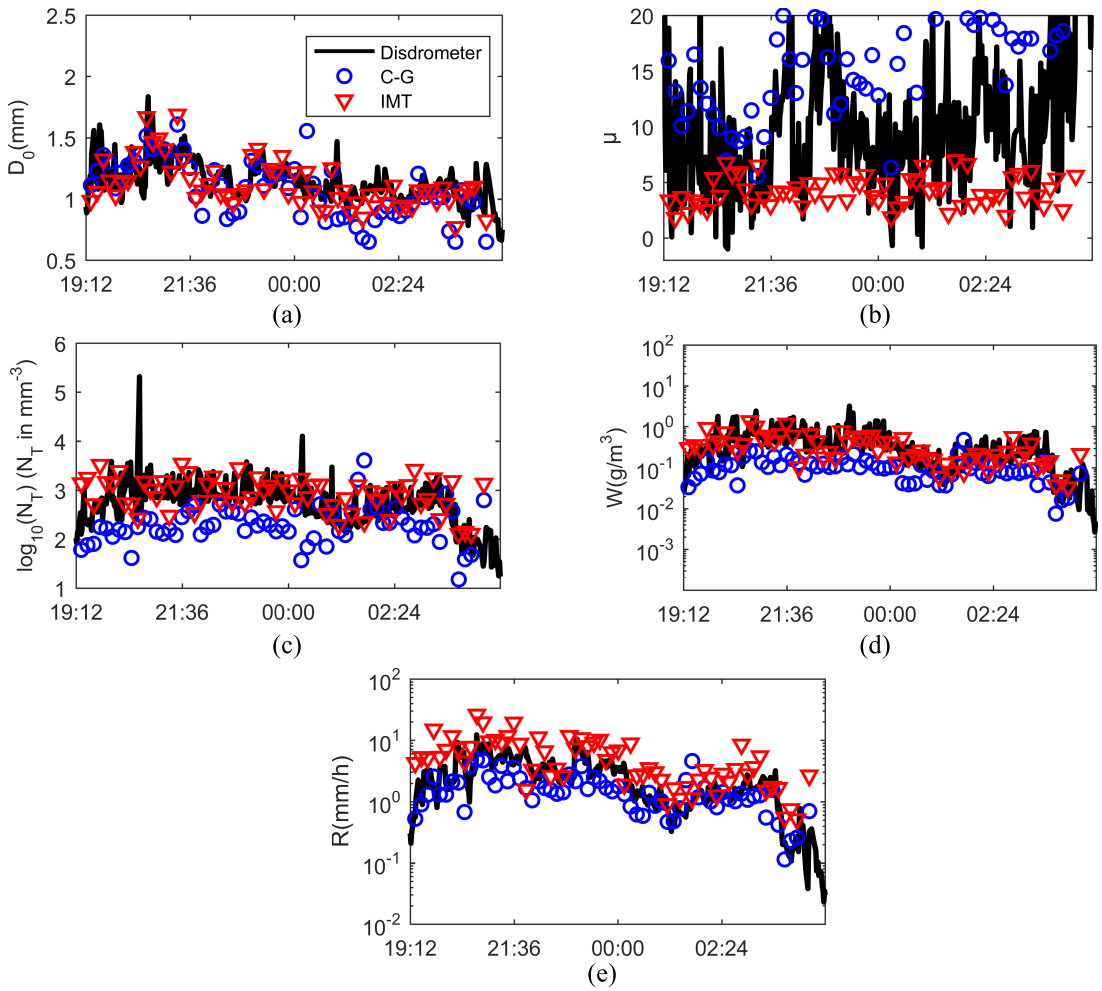

Fig. 13. Comparison of the three RSD parameters, water content and rainfall intensity between the observations and the results retrieved by the C-G and the IMT methods under real conditions in the large-scale rainfall event from 19:12 LST August 15 to 4:48 LST August 16, 2011.

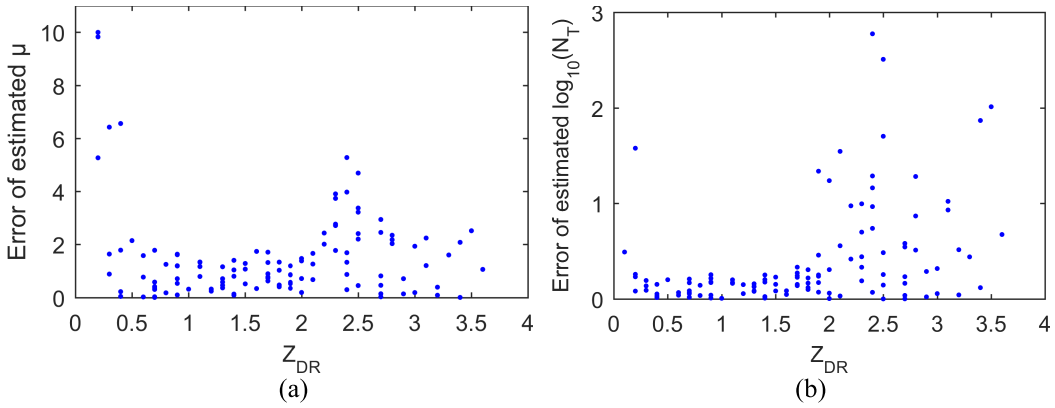

Fig. 14. Scatterplots of the retrieval errors versus Z_{DR}. (a) Retrieval error of μ versus Z_{DR}. (b) Retrieval error of $\log_{10}(N_T)$ versus Z_{DR}.

Figs. 2(e) and 3(b)]. The retrieval processes are related to the determination of μ, so inaccurate retrievals of μ can lead to inaccurate retrievals of $\log_{10}(N_T)$. However, not all samples with a Z_{DR} value lower than 0.3 dB or near 2.5 dB have large deviations. Therefore, there is still room for improvement in the treatment of nonmonotonic mapping situations. In general, this kind of situation only accounts for a small part of overall (Z_{H}, Z_{DR}). Using the retrieval scheme proposed in this article, the inverse mapping results of μ for most samples have an error less than 2, and the impacts of these errors on the general retrieval results are limited such as the results in Table IV.

B. Error Analysis of C-G Method

During the convective case illustrated in Section III, the C-G method produces a significant overestimation in W and R, although such situations did not appear in previous

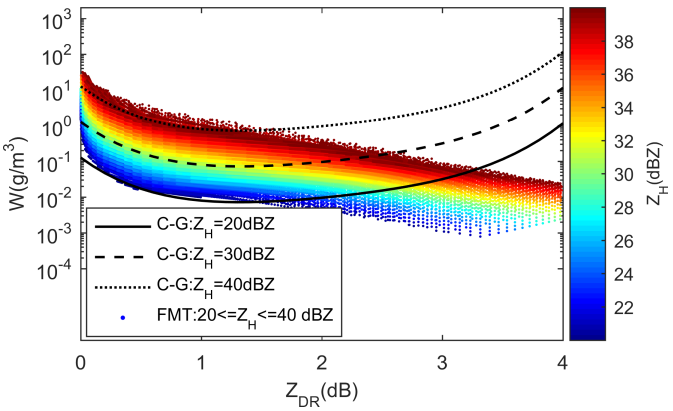

Fig. 15. Comparison of water content (W) from the FMT and calculated by C-G method. The lines are obtained by using Equation (17) at specific Z_{H} along the Z_{DR} range of 0–4 dB, and the color points are from FMT with 20 °C and Z_{H} values from 20 to 40 dBZ.

studies based on X-band dual-polarization radar using similar calculation schemes. In order to analyze these deviations, (17), which is used to obtain W, is assessed. When Li *et al.* [23] built calculation schemes for estimating RSD parameters [see (13)–(18)], they referred to (17) for W retrieval using X-band dual-polarization radar data from other studies including [10]. However, when Anagnostou *et al.* [10] introduced this empirical equation, they only referred to Brandes *et al.* [9], which is based on S-band radar. In addition, the details regarding how the high order polynomial of Z_{DR} in (17) was built was not provided. As a result, it is not easy to discuss the validation of form and parameters of (17). However, (17) can be compared with scattering simulation result when some variables such Z_{h} and temperature are fixed (see Fig. 15). The trends of W along Z_{DR} calculated by (17) is basically consistent with the scattering simulation shown by FMT where Z_{DR} is smaller than 1dB, but obviously larger than the FMT result when Z_{DR} is larger. One possible explanation is that, when Anagnostou *et al.* [10] built the fitting equation (17), most samples to fit the polynomial of Z_{DR} are with smaller Z_{DR}, so that the nonlinear trend of W along Z_{DR} can be matched well with smaller Z_{DR} but worse with higher Z_{DR}. Since W is overestimated, N_W will also be larger according to (18), leading to overestimation of both N_T and R.

Even the results and discussion do not indicate that the IMT method is always better than the C-G method since the schemes in (13)–(18) could be influenced by many factors such as fitting skills and fitting sample selection, the C-G method relies on empirical equations and there could be many other empirical schemes that are practical in different regions at different radar frequencies. The proposed IMT method does not rely on such nonlinear empirical relations and is more efficient.

C. Limitations of IMT Method

Although Section III demonstrates the applicability of the IMT method, there are still some limitations. Since the inverse mapping relies on differential phase variables, some conditions or observation regions without available differential phase measurements could make the IMT method not applicable. For example, in the boundary noise layer near the radar location, such as in the range of 0–8 km in Fig. 5, the observed Φ_{DP} cannot be easily filtered or smoothed to obtain the expected Φ_{DP} and K_{DP} of cloud and precipitation targets. In addition, near the edges of clouds, there may be large fluctuations in the differential phase. Therefore, the IMT method may not perform well in the regions near the radar location or under conditions when the precipitation clouds are weak/sporadic.

Another limitation of the proposed IMT method comes from the application of gamma-type RSD. The normalized gamma-type RSD (1) may not properly represent RSD when the measured RSD does not follow either an exponential distribution or a single peak distribution. The capability of disdrometers in measuring small and large raindrops [37]–[40] may also affect the development of a retrieval method, which limits the reliability of the obtained microphysical and precipitation variables such as N_T, W, and R. Previous studies attempted to improve the gamma model to achieve a better representation of RSD. For example, Thurai and Bringi [42] applied a generalized gamma model based on a double-moment normalization [43] and demonstrated a better representation of the shape parameter than the standard gamma form. Raupach *et al.* [44] introduced the reconstruction of RSD using double-moment normalization to obtain a better representation of RSD and rain-rate estimation for light rain. Nevertheless, there are more RSD parameters included in such gamma models. The way to retrieve those parameters using a limited number of radar observations still needs to be further investigated.

D. Sequences of Inverse Mapping

The mutually mapping relationships between RSD parameters and radar variables have been discussed, and one sequence of inverse mapping has been introduced in Section II. Theoretically, the sequence of inverse mapping can be exchanged. For example, (D_0, μ) and (Z_{H}, Z_{DR}) can also first be mutually mapped under similar processing with fixed N_T. Then the single layer of IMT with fixed N_T can be determined by differential phase variables. However, since the inverse mapping does not work well without differential phase measurements, the sequence of inverse mapping in Section II may be the most practical. Because when there are no available differential phase variables to determine μ, some empirical equations based on the ground observations, such as (13) and (16), can be the supplement for determination of μ. As a result, the layer in the IMT can be determined and three RSD parameters can also be retrieved.

VI. Conclusion

An IMT method has been proposed for retrieving RSDs using X-band dual-polarization radar data. Unlike previous studies that involve complicated semiempirical or empirical relationships based on ground observations, this IMT method directly establishes an inverse mapping database from polarimetric radar variables to RSD parameters. Based on the FMT constructed using the scattering model and the gamma-type RSD, the mapping relationships between certain RSD

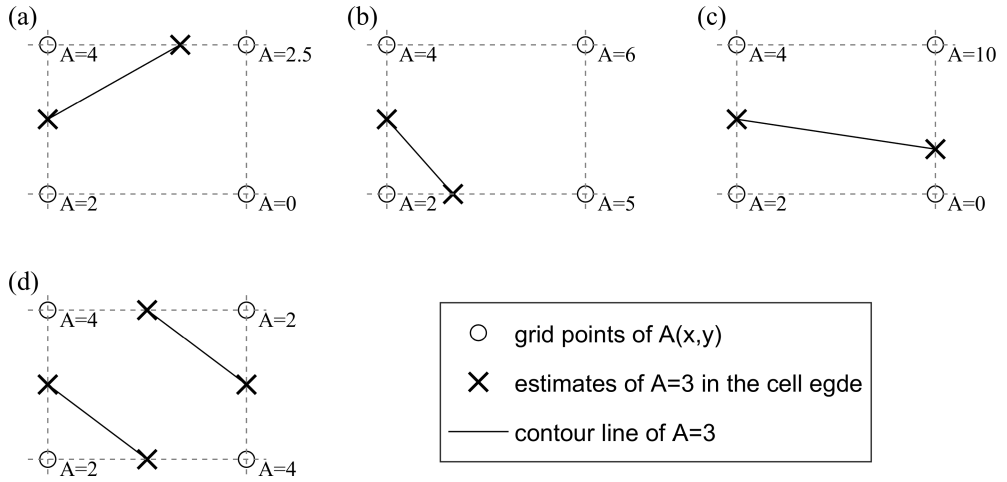

Fig. 16. Illustration of estimating contours in a grid cell. (a) Situation of three corner values less than the target value. (b) Three corner values are greater than the target value. (c) Two corner values are greater than the target value and axisymmetric distribution. (d) Two corner values are greater than the target value and centrosymmetric distribution.

parameters and polarimetric variables are determined by the intersection of contour lines and the monotonicity of different variables.

The C-G method for RSD parameter retrieval is selected for comparison. In the retrieval experiments under ideal conditions, the IMT method retrieved more reasonable results for all three gamma-type RSD parameters, D_0, N_T, and μ, as well as the water content and rainfall intensity compared to the C-G method, indicating the applicability of the IMT method in finding inverse mapping relationships between RSD parameters and polarimetric variables. In the noise sensitivity experiments, the IMT method generally is less sensitive to noise in reflectivity than the C-G method in D_0 and N_T retrievals and shows limited sensitivity to noise in differential phase variables. In the retrieval experiments during a real convective rainfall case, the C-G method shows large overestimation of W and R during severe convective rainfall periods, whereas the IMT method produces more reasonable results. While the performance of the two methods is similar in the large-scale continuous rainfall case, the IMT still produces slightly better D_0, N_T, and W retrievals.

Although more case studies are needed to further demonstrate the performance of the IMT method, the preliminary results show that the IMT method can be used to retrieve RSD parameters without long-term RSD observations or modeling complicated empirical relationships through nonlinear fitting of RSD parameters and radar measurements.

In future, more comprehensive noise sensitivity experiments can be designed to evaluate the IMT method under different conditions. Additionally, more retrieval methods could be compared and possibly combined since the IMT method does not work well when K_{DP} observations are missing.

APPENDIX

A. How to Obtain Contour Lines in Rectangular Cells

In the 2-D rectangular grid coordinates, a contour line is composed of a series of characteristic nodes and their connected segments. When drawing a contour figure, the computer has obtained the describing nodes of each contour, and many programming languages or software programs, such as MATLAB, IDL, or Surfer, can return these node data of each contour simultaneously. However, not all software has similar functions, so a simple method to obtain the nodes of contours in rectangular meshes is introduced below.

Assuming a variable A in coordinate (x, y), after specifying the value A_p of a contour line to be drawn, the basic steps are indicated as follows.

1) Estimate the position of $A = A_p$ on each edge of each mesh cell according to the corner value, and then, obtain all alternative nodes. When estimating the position of a node, different estimating methods can introduce some differences. For example, performing linear interpolation is faster, while spline interpolation can make the final contour smoother. Notice that no matter which estimation method is used, its accuracy is still determined by the grid spacing of the original cells. In this article, the method of linear interpolation is used.
2) Connect the alternative nodes mentioned above in a certain order and use the rules to form line segments across the cell. Contours can be divided into two categories according to the types of endpoints. One type is from the beginning of the coordinate system boundary to the end of the coordinate system boundary, and the other type is closure itself within the coordinate range. The former type usually proceeds first. Starting from the estimated position of an alternative node on one edge of a grid cell, if there is another alternative node on other edges, the two nodes are connected to obtain the line segment of the contour line in this cell, and then, we obtain the new search starting position [see Fig. 16(a)–(c)]. Since the contours are not intersecting in principle, it is a special case that all four edges of a grid cell have alternative nodes [see Fig. 16(d)]. In this case, it is necessary to specify that only the adjacent edges with smaller value corners, not the opposite edges or adjacent

edges with larger value corners, are connected. Another special case appears when the nodes are located on the corner point. Then, three alternative nodes may be met in this cell. In this case, the nodes located on the corner point should be ignored.

3) After determining all the contours starting from the boundary of the coordinate system, starting from any alternative node that has not been connected, the closure contours in the coordinate range will be successively determined until all the candidate nodes have been connected. Finally, one or more $A = A_p$ contours and their nodes can be obtained.

B. How to Obtain the Intersection of the Contour Lines From the Two Variables

Appendix A has shown that a contour line of a variable in a given value is expressed by a series of nodes and segments, so finding the intersection point of the two contour lines from the two variables can be accomplished by judging whether there is any intersection point between the two lines and finding the coordinates of that intersection point. Given the coordinates of four points $(x_{i,j},\ y_{i,j})$ $(j = 1, 2)$ in two line segments $i = 1, 2$, it is easy to obtain the analytic formula of the line corresponding to those two line segments. The coordinates of the intersection points of the two lines can be expressed by the following equation:

$$\begin{aligned} x_c &= (b_2 - b_1) / (a_2 - a_1) \\ y_c &= a_1 x_c + b_1 \end{aligned} \tag{B1}$$

where x_c and y_c are the coordinates of the intersection points of the two lines, a is the slope coefficient of a line, and b is the intercept coefficient of a line.

Then, we can judge whether there is any intersection between two lines simply by judging whether the intersections are on the two lines. The method for judging that is to sort x on each line segment in ascending order and then judge whether there is an intersection between the segments of the two lines to satisfy formula (B2). For some special cases where two lines are parallel, the result of (B1) will be infinite or incalculable, and formula B2 can also be judged as having no intersection

$$\begin{cases} x_{11} \le x_c \le x_{12} \\ x_{21} \le x_c \le x_{22}. \end{cases} \tag{B2}$$

By making judgments on all segments of the two contours from two variables, all possible intersections of the two contours can be obtained.

REFERENCES

[1] V. N. Bringi and V. Chandrasekar, *Polarimetric Doppler Weather Radar: Principles and Applications*. Cambridge, U.K.: Cambridge Univ. Press, 2001, doi: 10.1016/S0169-8095(02)00024-8.

[2] G. Zhang, *Weather Radar Polarimetry*. Boca Raton, FL, USA: CRC Press, 2016.

[3] A. V. Ryzhkov and D. S. Zrnic, *Radar Polarimetry for Weather Observations*. Cham, Switzerland: Springer, 2019, doi: 10.1007/978-3-030-05093-1.

[4] T. A. Seliga and V. N. Bringi, "Differential reflectivity and differential phase shift: Applications in radar meteorology," *Radio Sci.*, vol. 13, no. 2, pp. 271–275, Mar. 1978, doi: 10.1029/RS013i002p00271.

[5] G. Zhang, J. Vivekanandan, and E. Brandes, "A method for estimating rain rate and drop size distribution from polarimetric radar measurements," *IEEE Trans. Geosci. Remote Sens.*, vol. 39, no. 4, pp. 830–841, Apr. 2001, doi: 10.1109/36.917906.

[6] E. Gorgucci, V. Chandrasekar, V. N. Bringi, and G. Scarchilli, "Estimation of raindrop size distribution parameters from polarimetric radar measurements," *J. Atmos. Sci.*, vol. 59, pp. 2373–2384, Aug. 2002, doi: 10.1175/1520-0469(2002)059<2373:EORSDP>2.0.CO;2.

[7] J. Vivekanandan, G. Zhang, and E. Brandes, "Polarimetric radar estimators based on a constrained gamma drop size distribution model," *J. Appl. Meteorol.*, vol. 43, pp. 217–230, Feb. 2004, doi: 10.1175/1520-0450(2004)043<0217:PREBOA>2.0.CO;2.

[8] E. A. Brandes, G. Zhang, and J. Vivekanandan, "Comparison of polarimetric radar drop size distribution retrieval algorithms," *J. Atmos. Ocean. Technol.*, vol. 21, pp. 584–598, Apr. 2004, doi: 10.1175/1520-0426(2004)021<0584:COPRDS>2.0.CO;2.

[9] E. A. Brandes, G. Zhang, and J. Vivekanandan, "Drop size distribution retrieval with polarimetric radar: Model and application," *J. Appl. Meteor.*, vol. 43, pp. 461–475, Mar. 2004, doi: 10.1175/1520-0450(2004)043<0461:DSDRWP>2.0.CO;2.

[10] M. N. Anagnostou, E. N. Anagnostou, J. Vivekanandan, and F. L. Ogden, "Comparison of two raindrop size distribution retrieval algorithms for X-band dual polarization observations," *J. Hydrometeorol.*, vol. 9, no. 3, pp. 589–600, Jun. 2008, doi: 10.1175/2007jhm904.1.

[11] M. N. Anagnostou, J. Kalogiros, F. S. Marzano, E. N. Anagnostou, M. Montopoli, and E. Piccioti, "Performance evaluation of a new dual-polarization microphysical algorithm based on long-term X-band radar and disdrometer observations," *J. Hydrometeorol.*, vol. 14, no. 2, pp. 560–576, Apr. 2013, doi: 10.1175/JHM-D-12-057.1.

[12] Q. Cao, G. Zhang, and M. Xue, "A variational approach for retrieving raindrop size distribution from polarimetric radar measurements in the presence of attenuation," *J. Appl. Meteor. Climatol.*, vol. 52, pp. 169–185, Jan. 2013, doi: 10.1175/JAMC-D-12-0101.1.

[13] E. Yoshikawa, V. Chandrasekar, and T. Ushio, "Raindrop size distribution (DSD) retrieval for X-band dual-polarization radar," *J. Atmos. Ocean. Technol.*, vol. 31, pp. 387–403, Feb. 2014, doi: 10.1109/IGARSS.2012.6351005.

[14] E. Yoshikawa, V. Chandrasekar, T. Ushio, and T. Matsuda, "A Bayesian approach for integrated raindrop size distribution (DSD) retrieval on an X-band dual-polarization radar network," *J. Atmos. Ocean. Technol.*, vol. 33, no. 2, pp. 377–389, Feb. 2016, doi: 10.1175/JTECH-D-15-0060.1.

[15] G. Wen, H. Chen, G. Zhang, and J. Sun, "An inverse model for raindrop size distribution retrieval with polarimetric variables," *Remote Sens.*, vol. 10, no. 8, p. 1179, Jul. 2018, doi: 10.3390/rs10081179.

[16] C. W. Ulbrich, "Natural variations in the analytical form of the raindrop size distribution," *J. Climate. Appl. Meteor.*, vol. 22, pp. 1764–1775, Oct. 1983, doi: 10.1175/1520-0450(1983)022<1764:NVITAF>2.0.CO;2.

[17] P. T. Wills, "Functional fits to some observed drop size distributions and parameterization of rain," *J. Atmos. Sci.*, vol. 41, no. 9, pp. 1648–1661, May 1984, doi: 10.1175/1520-0469(1984)041<1648:FFTSOD>2.0.CO;2.

[18] M. I. Mishchenko, "Calculation of the amplitude matrix for a nonspherical particle in a fixed orientation," *Appl. Opt.*, vol. 39, no. 6, pp. 1026–1031, Feb. 2000, doi: 10.1364/AO.39.001026.

[19] V. N. Bringi, V. Chandrasekar, N. Balakrishnan, and D. S. Zrnić, "An examination of propagation effects in rainfall on radar measurements at microwave frequencies," *J. Atmos. Ocean. Technol.*, vol. 7, pp. 829–840, Dec. 1990, doi: 10.1175/1520-0426(1990)007<0829:AEOPEI>2.0.CO;2.

[20] E. Gorgucci, G. Scarchilli, V. Chandrasekar, and V. N. Bringi, "Measurement of mean raindrop shape from polarimetric radar observations," *J. Atmos. Sci.*, vol. 57, pp. 3406–3413, Oct. 2000, doi: 10.1175/1520-0469(2000)057<3406:MOMRSF>2.0.CO;2.

[21] E. Gorgucci, G. Scarchilli, V. Chandrasekar, and V. N. Bringi, "Rainfall estimation from polarimetric radar measurements: Composite algorithms immune to variability in raindrop shape–size relation," *J. Atmos. Ocean. Technol.*, vol. 18, pp. 1773–1786, Nov. 2001, doi: 10.1175/1520-0426(2001)018<1773:REFPRM>2.0.CO;2.

[22] Q. Cao, G. Zhang, E. A. Brandes, and T. J. Schuur, "Polarimetric radar rain estimation through retrieval of drop size distribution using a Bayesian approach," *J. Appl. Meteorol. Climatol.*, vol. 49, no. 5, pp. 973–990, May 2010, doi: 10.1175/2009JAMC2227.1.

[23] Z. Li, V. Chandrasekar, and T. Ushio, "Raindrop Size Distribution (DSD) retrieval for X-band dual-polarization radar," (in Chinese), *Climatic Environ. Res.*, vol. 20, no. 3, pp. 285–295, May 2015, doi: 10.3878/j.issn.1006-9585.2014.14021.

[24] C. F. Bohren and L. J. Battan, "Radar backscattering by inhomogeneous precipitation particles," *J. Atmos. Sci.*, vol. 37, pp. 1821–1827, Aug. 1980, doi: 10.1175/1520-0469(1980)037<1821:RBBIPP>2.0.CO;2.

[25] A. V. Ryzhkov, S. E. Giangrande, V. M. Melnikov, and T. J. Schuur, "Calibration issues of dual-polarization radar measurements," *J. Atmos. Ocean. Technol.*, vol. 22, no. 8, pp. 1138–1155, Aug. 2005, doi: 10.1175/JTECH1772.1.

[26] Q. Tang, H. Xiao, C. Guo, and L. Feng, "Characteristics of the raindrop size distributions and their retrieved polarimetric radar parameters in northern and southern China," *Atmos. Res.*, vols. 135–136, pp. 59–75, Jan. 2014, doi: 10.1016/j.atmosres.2013.08.003.

[27] E. A. Brandes, G. Zhang, and J. Vivekanandan, "An evaluation of a drop distribution–based polarimetric radar rainfall estimator," *J. Appl. Meteorol.*, vol. 42, no. 5, pp. 652–660, May 2003, doi: 10.1175/1520-0450(2003)042<0652:AEOADD>2.0.CO;2.

[28] E. Gorgucci, G. Scarchilli, and V. Chandrasekar, "A robust estimator of rainfall rate using differential reflectivity," *J. Atmos. Ocean. Technol.*, vol. 11, pp. 586–592, Apr. 1994, doi: 10.1175/1520-0426(1994)011<0586:AREORR>2.0.CO;2.

[29] E. Gorgucci, V. Chandrasekar, and G. Scarchilli, "Radar and surface measurement of rainfall during CaPE: 26 July 1991 case study," *J. Appl. Meteorol.*, vol. 34, no. 7, pp. 1570–1577, Jul. 1995, doi: 10.1175/1520-0450-34.7.1570.

[30] J. Hubbert and V. N. Bringi, "An iterative filtering technique for the analysis of copolar differential phase and dual-frequency radar measurements," *J. Atmos. Ocean. Technol.*, vol. 12, no. 6, pp. 643–648, 1995, doi: 10.1175/1520-0426(1995)012<0643:AIFTFT>2.0.CO;2.

[31] Y. Wang and V. Chandrasekar, "Algorithm for estimation of the specific differential phase," *J. Atmos. Ocean. Technol.*, vol. 26, no. 12, pp. 2565–2578, Dec. 2009, doi: 10.1175/2009JTECHA1358.1.

[32] L. Feng *et al.*, "Rain attenuation correction of reflectivity for X-band dual-polarization radar," *Atmosphere*, vol. 7, no. 12, p. 164, Dec. 2016, doi: 10.3390/atmos7120164.

[33] M. Löffler-Mang and J. Joss, "An optical disdrometer for measuring size and velocity of hydrometeors," *J. Atmos. Ocean. Technol.*, vol. 17, nos. 130–139, Feb. 2000, doi: 10.1175/1520-0426(2000)017<0130:AODFMS>2.0.CO;2.

[34] A. Kruger and W. F. Krajewski, "Two-dimensional video disdrometer: A description," *J. Atmos. Ocean. Technol.*, vol. 19, no. 5, pp. 602–617, 2002, doi: 10.1175/1520-0426(2002)019<0602:TDVDAD>2.0.CO;2.

[35] D. Atlas, R. C. Srivastava, and R. S. Sekhon, "Doppler radar characteristics of precipitation at vertical incidence," *Rev. Geophys.*, vol. 11, no. 1, p. 1, 1973, doi: 10.1029/RG011i001p00001.

[36] T. Kozu and K. Nakamura, "Rainfall parameter estimation from dual-radar measurements combining reflectivity profile and path-integrated attenuation," *J. Atmos. Ocean. Technol.*, vol. 8, pp. 259–270, Apr. 1991, doi: 10.1175/1520-0426(1991)008<0259:RPEFDR>2.0.CO;2.

[37] M. Thulai, W. A. Petersen, A. Tokay, C. Schultz, and P. Gatlin, "Drop size distribution comparisons between Parsivel and 2-D video disdrometers," *Adv. Geosci.*, vol. 30, pp. 3–9, May 2011, doi: 10.5194/adgeo-30-3-2011.

[38] A. Tokay, W. A. Petersen, P. Gatlin, and M. Wingo, "Comparison of raindrop size distribution measurements by collocated disdrometers," *J. Atmos. Ocean. Technol.*, vol. 30, no. 8, pp. 1672–1690, Aug. 2013, doi: 10.1175/JTECH-D-12-00163.1.

[39] T. H. Raupach and A. Berne, "Correction of raindrop size distributions measured by Parsivel disdrometers, using a two-dimensional-video-disdrometer as a reference," *Atmos. Meas. Techn. Discuss.*, vol. 7, no. 8, pp. 8521–8579, Aug. 2014, doi: 10.5194/amtd-7-8521-2014.

[40] S.-G. Park, H.-L. Kim, Y.-W. Ham, and S.-H. Jung, "Comparative evaluation of the OTT Parsivel2 using a collocated two-dimensional video disdrometer," *J. Atmos. Ocean. Technol.*, vol. 34, no. 9, pp. 2059–2082, Sep. 2017, doi: 10.1175/JTECH-D-16-0256.1.

[41] D.-S. Kim, M. Maki, and D.-I. Lee, "Retrieval of three-dimensional raindrop size distribution using X-band polarimetric radar data," *J. Atmos. Ocean. Technol.*, vol. 27, no. 8, pp. 1265–1285, Aug. 2010, doi: 10.1175/2010JTECHA1407.1.

[42] M. Thurai and V. N. Bringi, "Application of the generalized gamma model to represent the full rain drop size distribution spectra," *J. Appl. Meteorol. Climatol.*, vol. 57, no. 5, pp. 1197–1210, May 2018, doi: 10.1175/JAMC-D-17-0235.1.

[43] G. Lee, I. Zawadzki, W. Szyrmer, D. Sempere-Torres, and R. Uijlenhoet, "A general approach to double-moment normalization of drop size distributions," *J. Appl. Meteorol.*, vol. 43, pp. 264–281, Feb. 2004, doi: 10.1175/1520-0450(2004)043<0264:AGATDN>2.0.CO;2.

[44] T. H. Raupach, M. Thurai, V. N. Bringi, and A. Berne, "Reconstructing the drizzle mode of the raindrop size distribution using double-moment normalization," *J. Appl. Meteorol. Climatol.*, vol. 58, no. 1, pp. 145–164, Jan. 2019, doi: 10.1175/JAMC-D-18-0156.1.

Yue Sun was born in Beijing, China, in 1988. He received the B.S. degree in atmospheric science (weather modification direction) from the Nanjing University of Information Science and Technology, Nanjing, China, in 2011, and the M.S. degree in atmospheric physics and atmospheric environment from the Chengdu University of Information Technology, Chengdu, China, in 2016. He is pursuing the Ph.D. degree in atmospheric physics and atmospheric environment with the Institute of Atmospheric Physics, Chinese Academy of Sciences, Beijing, China.

From 2012 to 2016, he was engaged in statistical algorithm studying, numerical simulation, and software developing for artificial precipitation enhancement. Since 2015, he has participated in dual-polarization weather radar observations and experiments projects and mainly has been engaged in data processing, algorithm studying for cloud, and precipitation characteristics retrieving and applications. His research interests include dual-polarization radar meteorological algorithm research and applications, cloud precipitation physics, and numerical simulations.

Hui Xiao was born in Guangxi, China, in 1961. He received the B.S. degree in atmospheric physics from Nanjing University, Nanjing, China, in 1982, and the M.S. degree in atmospheric physics and the Ph.D. degree in meteorology from Graduate School, Chinese Academy of Sciences, Beijing, China, in 1985 and 2010, respectively.

During 1994–1996, he went to the Center for Global and Regional and Environmental Research (CGRER), University of Iowa, Iowa City, IA, USA, to conduct visiting research on the field of atmospheric environment. From 1996 to 2003, he was an Associate Professor with the Institute of Atmospheric Physics (IAP), Chinese Academy of Sciences (CAS), where he has been a Professor since 2004. He is a Professor with the University of Chinese Academy of Sciences, Beijing. From 1985 to 2000, his research was focused on the modeling simulation and observation of regionally atmospheric environment. Then, he is engaged in the numerical simulation and observation on cloud and precipitation physics, weather modification, and mesoscale weather systems. His recent research interests mainly include using X-band dual-polarization Doppler radar to detect strong convective systems, retrieving the hydrometeor distribution properties in clouds by using X-band radar observations, using disdrometer and micro-rain radar data to investigate precipitation properties, studying the characteristics of cloud microphysics and precipitation mechanism by numerical simulation, and using statistical method to evaluate precipitation enhancement effectiveness.

Dr. Xiao's awards and honors include once a second prize of the National Science and Technology Progress Award of China, twice the second prize of the Chinese Academy of Science's Natural Sciences Prize, and four times of the second prize of the provincial and ministry science and technology progress awards.

Huiling Yang was born in Ningxia, China, in 1983. She received the Ph.D. degree in atmospheric physics and atmospheric environment from the University of Chinese Academy of Sciences, Beijing, China, in 2011.

Since 2011, she has been an Associate Professor with the Institute of Atmospheric Physics, Chinese Academy of Sciences, Beijing. She is mainly engaged in the numerical simulation of mesoscale weather systems, the statistical analysis of cloud water resources and precipitation, comparison of cloud microphysical output in atmospheric models with hydrometeor classification based on X-band dual-polarization radar measurements for convective clouds and precipitation, and data analysis of raindrop spectrometer.

Liang Feng received the B.S. degree in electronic information engineering and the M.S. degree in signal and information processing from the Chengdu University of Information Technology, Chengdu, China, in 2006 and 2009, respectively, and the Ph.D. degree in atmospheric physics and atmospheric environment from the University of Chinese Academy of Sciences, Beijing, China, in 2018.

Since 2009, he has been an Engineer with the Institute of Atmospheric Physics, Chinese Academy of Sciences, Beijing, China. His research interests include dual-polarization radar meteorological applications and cloud precipitation physics.

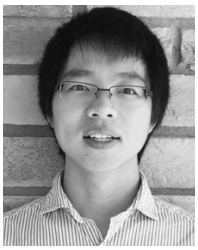

Haonan Chen (Member, IEEE) received the bachelor's degree from the Chongqing University of Posts and Telecommunications, Chongqing, China, in 2010, and the M.S. and Ph.D. degrees from Colorado State University (CSU), Fort Collins, CO, USA, in 2013 and 2017, respectively, all in electrical engineering.

He has been working with the Physical Sciences Division, NOAA/Earth System Research Laboratory, Boulder, CO, USA, since 2012, first as a Research Student, then a National Research Council Research Associate, and now a Radar, Satellite, and Precipitation Scientist through CIRA. He is also an Affiliate Faculty Member with the Department of Electrical and Computer Engineering, CSU. His research interest is mainly to advance the understanding of the physical sciences in the hydrometeorological processes using remote sensing technologies. He specializes in radar systems and networking, precipitation classification and estimation with polarimetric radar measurements, and multiscale radar and satellite data fusion.

Dr. Chen serves as an Associate Editor for the *Journal of Atmospheric and Oceanic Technology* and *URSI Radio Science Bulletin* and a Guest Editor for *Remote Sensing*.

Li Luo was born in Yibin, Sichuan, China, in 1990. She received the B.S. degrees in electronic information engineering from China West Normal University, Nanchong, China, in 2013, and the M.S. degree in agricultural informatization from the Chengdu University of Information Technology, Chengdu, China, in 2016. She is pursuing the Ph.D. degree in atmospheric physics and atmospheric environment with the Institute of Atmospheric Physics, Chinese Academy of Sciences, Beijing, China.

From 2014 to 2016, she studied the environment optimization of meteorological observation station at the Meteorological Observation Centre, China Meteorological Administration, Beijing, as a Visiting Graduate Student. She is the author of three articles. Her research interests include microphysical process analysis of clouds and precipitation, and weather radar data analysis and applications.